Properties of the open cluster Tombaugh 1 from high resolution spectroscopy and uvbyCaHβ photometry[1]

João V. Sales Silva[1,2], Giovanni Carraro[1,3], Barbara J. Anthony-Twarog[4], Christian Moni Bidin[5], Edgardo Costa[6] and Bruce A. Twarog[4]

1: ESO, Alonso de Cordova 3107, 19001, Santiago de Chile, Chile

2: Observatório Nacional/MCT, Rua Gen. José Cristino, 77, 20921-400, Rio de Janeiro, Brazil

3: On leave from Dipartimento di Fisica e Astronomia, Universitá di Padova, Italy.

4: Department of Physics and Astronomy, University of Kansas, Lawrence, KS 66045-7582, USA

5: Instituto de Astronomia, Universidad Católica del Norte, Av. Angamos 0610, Casilla 1280, Antofagasta, Chile

6: Departamento de Astronomia, Universidad de Chile, Casilla 36-D, Santiago, Chile

joaovictor@on.br,gcarraro@eso.org,bjat,btwarog[@ku.edu],

cmoni@ucn.cl,costa@das.uchile.cl

Received _____; accepted _____

ABSTRACT

Open clusters can be the key to deepen our knowledge on various issues involving the structure and evolution of the Galactic disk and details of stellar evolution because a cluster's properties are applicable to all its members. However the number of open clusters with detailed analysis from high resolution spectroscopy and/or precision photometry imposes severe limitation on studies of these objects.

To expand the number of open clusters with well-defined chemical abundances and fundamental parameters, we investigate the poorly studied, anticenter open cluster Tombaugh 1.

Using precision $uvbyCa\mathrm{H}\beta$ photometry and high resolution spectroscopy, we derive the cluster's reddening, obtain photometric metallicity estimates and, for the first time, present detailed abundance analysis of 10 potential cluster stars (9 clump stars and 1 Cepheid).

Using radial position from the cluster center and multiple color indices, we have isolated a sample of unevolved probable, single-star members of Tombaugh 1. From 51 stars, the cluster reddening is found to be $E(b-y) = 0.221 \pm 0.006$ or $E(B-V) = 0.303 \pm 0.008$, where the errors refer to the internal standard errors of the mean. The weighted photometric metallicity from m_1 and hk is [Fe/H] = -0.10 ± 0.02, while a match to the Victoria-Regina Strömgren isochrones leads to an age of 0.95 $\pm$ 0.10 Gyr and an apparent modulus of $(m - M) = 13.10$ $\pm$ 0.10. Radial velocities identify 6 giants as probable cluster members and the elemental abundances of Fe, Na, Mg, Al, Si, Ca, Ti, Cr, Ni, Y, Ba, Ce, and Nd have been derived for both the cluster and the field stars.

Tombaugh 1 appears to be a typical inner thin disk, intermediate-age open cluster of slightly subsolar metallicity, located just beyond the solar circle, with

solar elemental abundance ratios except for the heavy s-process elements, which are a factor of two above solar. Its metallicity is consistent with a steep metallicity gradient in the galactocentric region between 9.5 and 12 kpc. Our study also shows that Cepheid XZ CMa is not a member of Tombaugh 1, and reveals that this Cepheid presents signs of barium enrichment, making it a probable binary star.

Subject headings: stars: abundances - open clusters and associations: general - open clusters and associations: individual: Tombaugh 1 - stars: atmospheres

1. Introduction

Tombaugh 1 is a star cluster in the Canis Majoris constellation at $\alpha = 07^h00^m29^s$, $\delta = -20^o34'00''$, and $\ell, b = 232°.22, -7°.32$ (2000.0 equinox), discovered in 1938 by Clyde Tombaugh (Tombaugh 1938). A quick glance at any sky image shows only a small enhancement of stars in a rich Galactic field, a primary reason why Tombaugh 1 has been studied very little until now. As detailed in Sect. 2, estimates of its fundamental parameters vary strongly from author to author, photometric data are scanty, and spectroscopic data totally absent.

There are, however, several reasons to consider this cluster particularly interesting. With a Galactic latitude of $-7^o.32$ and an assumed a distance of 2–3 kpc (Piatti et al. 2004; Carraro & Patat 1995), Tombaugh 1 is situated ∼300–400 pc below the Galactic plane, a location rare among open clusters of the presumed age of Tombaugh 1 ($\lesssim 10^9$ yr). The direction to Tombaugh 1 intersects the Perseus and Orion arms in the third Galactic quadrant, and the cluster was for some time associated with the putative Canis Major dwarf galaxy (Bellazzini et al. 2004). Although the discussion of this topic has been dormant for some time (Carraro et al. 2008), it would still be valuable to determine the cluster distance with enough precision to associate it with either the Perseus or, possibly, the Orion arm extension in the third Galactic quadrant (Vásquez et al. 2008). Moreover, a distance of 2–3 kpc places Tombaugh 1 at a galactocentric distance of 10–11 kpc, a location where some observations indicate an abrupt change in the abundance gradient of the disk (see, e.g. Twarog et al. 1997; Lepine et al. 2011). Improved cluster distance and metallicity estimates would be of paramount importance in probing this picture of the outer Galactic disk chemical properties. Metallicity, in particular, has never been measured reliably, but

[1]Based on observations carried out at Las Campanas Observatory (program ID: CN2009B-042) and Cerro Tololo Inter-American Observatory.

only inferred either from photometric indices or via comparison with isochrones (Piatti et al. 2004).

With these goals in mind, we present new Strömgren $uvbyCa\mathrm{H}\beta$ photometry for a large field around the cluster and high resolution spectroscopy of 10 potential cluster stars (9 red giant clump stars and 1 Cepheid). This unique dataset will be used to provide precise estimates of the cluster basic parameters, in particular, reddening, distance, age, overall and elemental metallicity.

The paper is organized as follows: Section 2 gives details on the limited investigation of the cluster to date. In Section 3 we present the photometric and spectroscopic observations and their reduction, as well as a description of the radial-velocity determinations for membership. Section 4 details the derivation of the cluster properties from photometry, while Section 5 is devoted to the spectroscopic abundance analysis. In Section 6 we discuss the results of our spectroscopic analysis in detail. Section 7 interprets Tombaugh 1 in the context of galactic evolution and summarizes our findings.

2. Tombaugh 1: Background

Tombaugh discovered Tombaugh 1 and Tombaugh 2 during the trans-Neptunian planet search at Lowell Observatory (Tombaugh 1938, 1941), reporting an apparent diameter for Tombaugh 1 of $\sim 5'$, with typical cluster stars having a visual magnitude of 14-15. His short description of the cluster notes that the field in the direction of Tombaugh 1 is extremely rich, suggesting that this might be the reason why the cluster went undetected for so long.

As discussed in Turner (1983); Haffner (1957) and Tifft (1959) independently rediscovered Tombaugh 1, reporting discrepant values for the cluster declination; the Haffner (1957) position is incorrect. Tifft (1959) noted the cluster because the Cepheid

XZ CMa lies about one cluster diameter northward of the cluster center. Turner (1983) provided the first estimates for the cluster fundamental parameters from analysis of UBV photoelectric photometry of 26 stars, including 5 likely members and 10 possible members selected by radial location in the cluster and position in the two-color diagram, the UBV diagram also indicating $E(B-V) = 0.27 \pm 0.01$ mag. Turner (1983) measured a cluster diameter of $\sim 10'$ and estimated a distance and age of 1.26 kpc ($(m-M) = 11.34 \pm 0.04$) and ∼800 Myr, respectively, using the Hyades cluster adjusted to solar metallicity as a reference, though the sparse photometry extended barely 1.5 mag below the top of the turnoff. Lastly, Turner (1983) suggested that Tombaugh 1 hosts a probable blue straggler star (BSS), later confirmed by Ahumada & Lapasset (1995).

Turner (1983) also investigated the membership of Cepheid XZ CMa with Tombaugh 1. Turner suggested that XZ CMa is not a member of Tombaugh 1. However, this conclusion was never subjected to a more rigorous analysis based in high-resolution spectroscopy. So, we also analyzed spectroscopically XZ CMa to confirm or exclude the cluster membership. In fact, cluster Cepheids are important to fix the distance scale (see e.g., Majaess et al. 2013a; Majaess et al. 2013b).

The first CCD study of Tombaugh 1, limited to VI, was carried out by Carraro & Patat (1995), covering an area $6'$ on a side, essentially the cluster core (Turner 1983). Very different values for some of the cluster basic parameters were found: reddening, distance, and age of $E(B-V) = 0.40 \pm 0.05$, 3 kpc ($(m-M) = 13.60 \pm 0.2$), and 1 Gyr, respectively, tied to color-magnitude diagram (CMD) matches to theoretical isochrones. While this study dealt with only two filters and field star contamination makes it difficult to identify the cluster turnoff clearly, the parameter differences are not unexpected given the sparse sample of the earlier study.

Piatti et al. (2004) presented a more extensive CCD study using Washington

photometry, covering a large area around the cluster. The cluster was found to be 1.3 Gyr old from a combination of CMD morphology and isochrone fits, assuming [Fe/H] = −0.40, with distance and reddening estimates intermediate between the Turner (1983) and Carraro & Patat (1995) values. An attempt was also made to directly measure the metallicity using Washington photometry, obtaining [Fe/H] = −0.30 with a large uncertainty of ±0.25 dex.

Finally, on the basis of stellar data from PPMXL[2] and 2MASS, Kharchenko et al. (2013) obtained some spatial, structural, kinematic, and astrophysical parameters of Tombaugh 1. In particular, they determined for Tombaugh 1 an age of 1.16 Gyr, a reddening $E(B-V) = 0.281$ and a distance of 2642 pc ($(m-M) = 12.98$), values similar to those obtained by Piatti et al. (2004). Kharchenko et al. (2013) also estimated average proper motion in right ascension (−0.99 mas/yr) and in declination (3.97 mas/yr), but didn't estimate the average radial and galactic space velocities of Tombaugh 1.

3. Observations and Data Reduction

3.1. Photometry

Photometry for Tombaugh 1 was secured in December 2010, during a 5-night run using the Cerro Tololo Inter-American Observatory 1.0m telescope operated by the SMARTS consortium[3]. The telescope is equipped with an STA 4064 × 4064 CCD camera[4] with 15-μm pixels, yielding a scale of 0.289″/pixel and a field-of-view (FOV) of 20′ × 20′ at the Cassegrain focus of the telescope.

---

[2]PPMXL is a catalog of positions, proper motions, 2MASS, and optical photometry of 900 million stars and galaxies. For more information: `http://vo.uni-hd.de/ppmxl`

[3]`http://http://www.astro.yale.edu/smarts`

[4]`http://www.astronomy.ohio-state.edu/Y4KCam/detector`

In Table 1 we present the log of our Strömgren observations, together with exposure times and airmasses. A total of 75 images were acquired for Tombaugh 1. All observations were carried out under photometric conditions with good-seeing (0.8–1.2 arc sec). A sample image of the covered field is shown in Fig. 1.

Basic calibration of the CCD frames was done using the Yale/SMARTS y4k reduction script based on the IRAF[5] package CCDRED, and the photometry was performed using IRAF's DAOPHOT and PHOTCAL packages. Instrumental magnitudes were extracted following the point spread function (PSF) method (Stetson 1987) using a quadratic, spatially-variable master PSF (PENNY function). Finally, the PSF photometry was aperture-corrected using corrections determined from aperture photometry of bright, isolated stars in the field.

Standard stars for the extended Strömgren system were observed on one of the photometric nights on which Tombaugh 1 was observed. We additionally employed observations of secondary standard fields in several open clusters, using the same telescope and instrument one year later, to derive the form of the calibration equations. The clusters observed in December 2011 were M67 (Nissen et al. 1987), NGC 2287 (Schmidt 1984) and NGC 2516 (Snowden 1975). The zeropoint for each calibration equation applied to Tombaugh 1 was anchored by observations of eight field star standards obtained on 7 December, 2010. Standard values were obtained from the catalogs of Olsen (1983, 1993, 1994) for *uvby*, from Hauck & Mermilliod (1998) for Hβ values and from Twarog & Anthony-Twarog (1995) for *hk* index values for the field star standards.

---

[5]IRAF is distributed by the National Optical Astronomy Observatory, operated by the Association of Universities for Research in Astronomy, Inc., under cooperative agreement with the National Science Foundation.

Table 2 summarizes the calibration equations' slopes and color terms. Following a standard practice for Strömgren photometry, calibration of $(b-y)$ would require that separate slopes be determined for cooler dwarfs as distinct from warmer dwarfs and giants. Insufficient cool dwarf standards were observed to accomplish this. The slope listed in Table 2 is appropriate for giants and dwarfs with $(b-y)_0 \leq 0.42$; application of this slope to dwarfs redder than this is an unavoidable extrapolation. Bluer dwarfs represent the only class for which m_1 and c_1 calibrations could be established with any confidence. The errors listed in Table 2 represent the standard deviation of the calibrated values about the standard values for the field star standards, indicating the external precision of the zeropoints of the calibration equations. The final calibrated catalog was then cross-correlated with 2MASS to convert pixel (i.e., detector) coordinates into RA and DEC for J2000.0 equinox, thus providing 2MASS-based astrometry. An excerpt of the optical photometric table used in this investigation is illustrated in Table 3. Fig. 2 shows the trend of errors with V magnitude. The V and $b-y$ data remain below 0.02 mag uncertainty to the limit of Table 3 ($V = 18.5$), while errors in the remaining indices begin to rise above this value at $V =$ 16.5, 17.25, 17.25, and 17.5 for c_1, m_1, hk, and Hβ, respectively.

3.2. Spectroscopy and Radial Velocities

Over the night of January 5, 2010, we observed ten potential cluster stars (nine clump stars and one Cepheid, see Sec. 4.1) with the *Inamori-Magellan Areal Camera & Spectrograph* (IMACS, Dressler et al. 2006) attached to the Magellan telescope (6.5 m) located at Las Campanas, Chile. The spectra were obtained using Multi-Object Echelle (MOE) mode with two exposures, one of 900s and other of 1200s. Our spectra have a resolution of R$\sim$20000, while the spectral coverage depends on the location of the star on the multi-slit mask, but generally goes from 4200 Å to 9100 Å. The detector consists of a

mosaic with eight CCDs with gaps of about 0.93 mm between the CCDs, causing small gaps in stellar spectra.

The spectra were reduced following the standard procedures using IRAF, which includes CCD bias and flat-fielding correction, spectrum extraction, wavelength calibration and sky subtraction using the tasks CCDPROC, DOECSLIT, ECIDENTIFY and BACKGROUND, respectively. For each CCD, we performed bias and flat-fielding correction separately, after which we used the IRAF tasks IMCREATE and IMCOPY to join the CCDs and create the mosaic. The cosmic rays were removed with the IRAF Laplacian edge-detection routine (van Dokkum 2001), and the radial velocities were obtained from the wavelength shift of the unblended absorption lines of Fe covering the entire wavelength range. The values of wavelength shift were measured via line-by-line comparison between observed and laboratory wavelength with the lines center of observed wavelength being determined through the task SPLOT in IRAF. To derived the final radial velocities we applied a zero-point offset correction using the task FXCOR in IRAF to cross-correlate the telluric lines of the observed spectra with telluric lines of the high-resolution FEROS solar spectrum collected by us in a previous run (Moni Bidin et al. 2012). To calculate the heliocentric velocities and combine the spectra of different exposures, we used the IRAF tasks RVCORRECT and SCOMBINE, respectively. We took the stars heliocentric radial velocity to be the average of the two epochs measured and the error to be the difference between the two values multiplied by 0.63 (small sample statistics; see Keeping 1962). The nominal S/N ratio was evaluated by measuring with IRAF the rms flux fluctuation in selected continuum windows. The values at 6000 Å are shown in Table 4.

Table 4 gives some information about the observed stars: IDs (Carraro & Patat 1995), right ascension, declination, V and $b-y$ from Table 3 and $V-I$ photometry (Carraro & Patat 1995), heliocentric radial velocities (RV_1 and RV_2) at two epochs and their mean

values ($\langle$RV$\rangle$), projected rotational velocities (vsini) and spectral signal-to-noise at 6000 Å. We estimated the projected rotational velocities, vsini, by a spectral synthesis technique using unblended Fe lines analyzed with model atmospheres, a macroturbulent velocity of 3 km s^{-1}, limb darkening and instrumental broadening corresponding to IMACS spectral resolution. For some stars with low vsini it was possible to determine only an upper limit because of the insensitivity of the spectral synthesis to vsini below 2.7 km s^{-1} .

In the literature, there is no information about the radial velocity of Tombaugh 1. So, to determine the membership of stars, we first found for a group of stars with similar heliocentric radial velocities (RV) in the sample, to have a preliminary cluster radial velocity and a list of members, that could be iteratively refined. The stars with RV within 2σ of the cluster mean heliocentric radial velocity were classified as member of Tombaugh 1. The membership of the Cepheid XZ CMa (star 806) was not defined by its heliocentric radial velocity, because its RV is variable due to pulsations. So, we classified XZ CMa as non-member of Tombaugh 1 because its metallicity ([Fe/H]=-0.53) is much lower than metallicity of stars classified as member of Tombaugh 1 (see Table 9). We identify six red clump giants belonging to Tombaugh 1 and derive a mean cluster heliocentric radial velocity of 81.1 $\pm$ 2.5 km s^{-1}.

4. Cluster Parameters from Photometry

As discussed previously, one of the primary challenges in identifying and studying Tombaugh 1 is isolating the moderately populated cluster from the rich stellar background. This is particularly important for defining directly the fundamental cluster parameters of reddening and metallicity and indirectly the distance and age. The challenge is illustrated in Fig. 3, where the $V, b-y$ CMD for the entire field of study is presented. Red giants observed as part of this investigation and found to be probable radial-velocity members are plotted as

red starred points; probable nonmember are open red triangles. The complexity of the stellar population mix in this region of the galaxy is evident and will be discussed in detail in a future paper. To enhance our definition of the cluster, we first reinvestigate the radial profile of the cluster.

4.1. Star Counts and Cluster Size

To quantify the amount of field star contamination, we performed star counts to derive an estimate of the cluster center and size. Using an array of positions covering the field of the CCD, we derived a density contour map and calculated the density inside each grid step by a kernel estimate (Carraro et al. 2014c). This is shown in Fig. 4, which confirms the appearance of Fig. 1 that Tombaugh 1 is far from being a symmetric object. The cluster looks elongated in the direction NE to SW, and the highest peak does not represent the center of a uniform star distribution. The largest peak is located at RA = $105^o.11$, DEC = $-20^o.58$, while the nominal center of the cluster is clearly displaced to the northeast direction at RA = $105^o.13$, DEC = $-20^o.54$. The loose and irregular shape of Tombaugh 1 may be the result of its dynamical evolution due to its tidal interaction with the Milky Way. However, little kinematic information beyond the cluster radial velocity exists to confirm this scenario. High quality proper motions could go a long way to defining the direction of the cluster motion and test if this coincides with the direction of the apparent cluster deformation, indicating if Tombaugh 1 has indeed been tidally disturbed.

To isolate probable cluster members, assumed to be those stars which lie within the cluster boundaries, we derive the cluster radial surface density profile shown in Fig. 5. This has been computed by drawing concentric rings centered on the nominal cluster center. This is motivated by the fact that, while the densest central regions look distorted, the cluster halo still retains a more spherical profile. Star counts level off at $\sim 4'$ from the

cluster nominal center, close to the value reported by Turner (1983). The mean density in the field surrounding the cluster is 5 stars/arcmin^2 (see also Fig. 4), and our survey covers the whole cluster area. As a consequence, in the following we will adopt $4'$ as the cluster radius and refer to this area as the cluster area, while the area outside $4'$ from the cluster center will be referred to as the offset field.

4.2. Photometric Reddening and Metallicity

In the absence of membership information for any stars beyond those in Table 4, we can enhance the likelihood of including cluster members in our sample by restricting the analysis to stars within $3.5'$ of the cluster center, just short of the transition region from the cluster to the field based upon star counts. Fig. 6 shows the $V, b-y$ CMD for stars within this core; all red giant members, independent of radial location, are plotted as stars, while open triangles are probable nonmembers. The cluster's turnoff region and the blue edge of the main sequence are well-defined to the limit of the survey. The color spread at the top of the turnoff and the color and magnitude differential between the turnoff and the giant branch are very reminiscent of NGC 5822, a cluster of slightly subsolar metallicity with an age of 0.9 Gyr (Carraro et al. 2011). An additional means of demonstrating the cluster population comes from the V, hk CMD for the core region, shown in Fig. 7. In the likely probability that there is a modest reddening range across the face of the cluster, this CMD minimizes the impact due to the weak sensitivity of hk to reddening but a strong sensitivity to temperature and metallicity changes, factors we will make effective use of below. The tight vertical band defining the cluster turnoff reflects this fact, while the steep slope in V with hk is indicative of the cluster age; the trend in hk with decreasing $b-y$ plateaus as the stellar sample moves from F to A stars, leading to an almost vertical turnoff in the V, hk CMD for clusters of intermediate age, as illustrated by NGC 5822 in Fig. 13 of Carraro et

al. (2011). Among the giants, the positions of the two faintest radial-velocity members, 663 and 1349, place them redward of the majority of the probable clump stars and indicates that, despite their similar velocities, they are probable field stars. In the absence of more information, they will be retained in the discussions below.

To further isolate probable members for defining the reddening and metallicity, we restrict our sample to stars populating the blue edge of the cluster main sequence between $V = 15.50$ and 17.0. The bright cutoff eliminates the evolved stars that populate the color spread at the top of the main sequence while the faint boundary defines the magnitude range where errors in the color indices begin to increase for m_1, hk, and especially c_1. The blue edge of the main sequence in this magnitude range was used to define a single-star boundary and any star within ∼0.4 mag of the boundary was classified as a single star (blue circles in Fig. 8). Stars between 0.4 and 0.8 mag were classed as probable binaries (black squares in Fig. 8), if members, while all stars more than 0.8 mag beyond the main sequence were tagged as likely field stars (red crosses in Fig. 8).

We can check this classification using the V, hk CMD of Fig. 9. Stars can be located off the main sequence for a variety of reasons: bad and/or contaminated photometry, binarity, excessive reddening compared to the typical cluster star and/or nonmembership. As noted earlier, the hk index is very sensitive to color changes due to temperature and only weakly impacted by reddening. In fact, increased reddening moves a star blueward in hk. As shown in Fig. 9, the separation by class as defined by Fig. 8 is well corroborated. With only four obvious exceptions, the single stars form a well-defined turnoff band covering a modest range in hk. The stars redward of the main sequence band in Fig. 9 are dominated by the stars tagged as redder in Fig. 8, indicating that these are truly redder than the cluster sequence and that the majority are probable nonmembers. Three red crosses which sit on the main sequence in Fig. 9 deserve some explanation. These are either highly reddened

field stars or, more likely, field stars in the direction of the cluster with significantly lower metallicity than Tombaugh 1. For metallicity and reddening estimation, we will limit the sample to the single stars (blue circles), with the four points which deviate from the cluster main sequence in Fig. 9 excluded.

For consistency with past cluster work, we will derive the reddening from two Strömgren relations from Olsen (1988) and Nissen (1988), a slightly modified version of the original relations derived by Crawford (1975, 1979). Reddening estimates are derived in an iterative fashion. The indices are corrected using an initial guess at the cluster reddening and the intrinsic $b-y$ is derived using the reddening-free Hβ adjusted for metallicity and evolutionary state. A new reddening is derived by comparing the observed and intrinsic colors and the procedure repeated. The reddening estimate invariably converges after 2–3 iterations. To derive the reddening, one needs to correct $b-y$ for metallicity, so a fixed [Fe/H] is adopted for the cluster and the reddening derived under a range of [Fe/H] assumption that bracket the final value. The complementary procedure is to vary the mean reddening value for the cluster and derive the mean [Fe/H]. Ultimately, only one combination of $E(b-y)$ and [Fe/H] will be consistent.

For Tombaugh 1, the metallicity from m_1 was varied between [Fe/H] = -0.28 and $+0.12$, generating a range of $E(b-y) = 0.224$ to 0.214 for the relation of Olsen (1988) and 0.223 to 0.216 for Nissen (1988) from 51 stars within the Hβ calibration range. In all cases, the standard error of the mean for the final $E(b-y)$ is $\pm$ 0.006 mag. For [Fe/H] from m_1 equal to -0.16, the reddening from the two relations is virtually identical at $E(b-y) = 0.221 \pm 0.006$; the difference between the two reddening values is statistically insignificant compared to the standard errors of the mean. If $E(b-y) = 0.73^{*}E(B-V)$, the reddening estimate from Strömgren data alone is $E(B-V) = 0.303 \pm 0.008$. There is weak evidence for a variation in $E(b-y)$ across the face of the cluster, with the reddening being higher on

average by 0.03 mag in the southwest and lower by a comparable amount in the northeast. Without more membership information, for purposes of deriving the cluster parameters, we will adopt the cluster mean for all stars.

With the reddening set, we can derive the metallicity from both m_1 and hk, using Hβ as the primary temperature index. From 51 stars, [Fe/H] = -0.165 ± 0.027 from m_1 and -0.086 ± 0.013 from hk. If one anomalous measurement located more than three sigma from the cluster mean is removed from the m_1 analysis, the revised [Fe/H] becomes -0.153 ± 0.025. The greater uncertainty in the metallicity estimate from m_1 relative to hk is a reflection of the greater sensitivity of m_1 to reddening changes and a lower sensitivity to metallicity variation; the small difference in [Fe/H] can be entirely explained by a zero-point offset of 0.005 mag in m_1. Weighting the two photometric estimates by the inverse square of the errors leads to a final value of [Fe/H] = -0.10 ± 0.02.

4.3. Age and Distance Estimation

One of the rare sets of available isochrones which include models transformed to the Strömgren system is the Victoria-Regina (VR) set of isochrones (VandenBerg et al. 2006). Fig. 10 shows the scaled-solar models for [Fe/H] = -0.11, ages 0.8, 0.9, and 1.0 Gyr, adjusted for $E(b-y) = 0.221$ and $(m-M) = 13.10$. Symbols have the same meaning as in Fig. 6. The already noted similarity of Tombaugh 1 to NGC 5822 is confirmed. In addition to the similar scatter in $b-y$ at the top of the turnoff, the best fit age estimate is between 0.9 and 1.0 Gyr; the best fit to a different set of broad-band isochones for NGC 5822 produced an age of 0.9 ± 0.1 Gyr for the more populated cluster (Carraro et al. 2011). The reddening-corrected true distance modulus is $(m-M)_o = 12.15$, in excellent agreement with the most recent work of Kharchenko et al. (2013).

5. Atmospheric Parameters and Abundances Analysis

The equivalent width measurements of absorption lines of Na, Mg, Al, Si, Ca, Ti, Cr, Ni and Fe were used to obtain their respective chemical abundances while the abundances of Y, Ba, Ce and Nd were derived through spectral synthesis. The equivalent widths were measured manually using the task SPLOT in IRAF to fit a Gaussian profile to the observed absorption line. We rejected the absorption lines with equivalent widths greater than 160 mÅ because these lines are saturated, which prevents a Gaussian fit to the absorption lines (Pereira et al. 2011). All equivalent widths used to obtain the atmospheric parameters and chemical abundances are shown in the Tables 5, 6, 7 and 8.

The atomic-line list adopted in this work is the same as the one used by Santrich et al. (2013) and Sales Silva et al. (2014). For Ba II line, the hyperfine structure (HFS) was taken into account and we used the line list of Carraro et al. (2014b). In Tables 5 and 6 we describe the line list with excitation potential (ξ) and oscillator strength (gf) for absorption lines of Fe I and Fe II. The values of the oscillator strength adopted for the Fe I and Fe II lines were taken from Lambert et al. (1996) and Castro et al. (1997). Tables 7 and 8 show the atomic parameters (gf and ξ values) of the absorption lines of the elements Na, Mg, Al, Si, Ca, Ti, Cr and Ni with their respective references (column 5). Atomic parameters for several transitions of Ti, Cr, and Ni were retrieved from the National Institute of Science and Technology Atomic Spectra Database (Martin et al. 2002). For Na we used only two absorption lines, 6154.226 Å and 6160.747 Å. These Na lines have a clean profile which makes it possible to calculate the chemical abundance of Na through the equivalent width (Smiljanic 2012). The absorption lines used to obtain s-process elements abundances were 5289 Å and 5402 Å for Y, 5853 Å for Ba, 5117 Å and 5187 Å for Ce and 4914 Å for Nd.

The atmospheric parameters and chemical abundances were obtained in the same manner as in Pereira et al. (2011), Santrich et al. (2013), and Sales Silva et al. (2014)

using the local thermodynamic equilibrium (LTE) model atmospheres of Kurucz (1993) and the spectral analysis code MOOG (Sneden 1973). Excitation equilibrium was used to derive the effective temperature ($T_{\rm eff}$) as defined by a zero slope of the trend between the iron abundance derived from Fe I lines and the excitation potential of the measured lines. Microturbulent velocity was adjusted until both the strong and weak Fe I lines (represented by reduced equivalent width, W_λ/λ) gave the same abundance. Finally, the surface gravity was determined using the ionization equilibrium found from the equality of the abundances of Fe I and Fe II. The final adopted atmospheric parameters are given in Table 9.

The uncertainty in the slopes of the Fe I abundance versus excitation potential and Fe I abundance versus reduced equivalent width were used to derive the uncertainties in our adopted effective temperatures ($T_{\rm eff}$) and microturbulent velocities (ξ), respectively. The standard deviation in $\log g$ was set by changing this parameter around the adopted solution until the difference between Fe I and Fe II mean abundance differed by exactly one standard deviation of the [Fe I/H] mean value. We estimated typical uncertainties in atmospheric parameters of the order of $\pm 180\,{\rm K}$, ± 0.3 dex, and ± 0.3 km s^{-1} for $T_{\rm eff}$, $\log g$ and ξ, respectively.

We also calculated the photometric effective temperature and photometric gravity to compare with our spectroscopic temperature and gravity. Photometric temperatures were calculated using the calibration of Alonso et al. (1999) and our values of $(b-y)$ with $E(b-y) = 0.221$. The photometric gravity for each star was obtained from the equation:

$$\begin{aligned} \log g_\star &= \log \frac{M_\star}{M_\odot} + 0.4\,(V - A_V + BC) \\ &\quad + 4 \log T_{\rm eff} - 2 \log r\ ({\rm pc}) - 10.62. \end{aligned} \tag{1}$$

Where T_{eff} is the photometric effective temperature and M is the mass. Based upon the

VR isochrones and an age of 0.95 Gyr, the typical mass for a star in the color range of the likely member red giants is $2.15 M_{\odot}$. The photometric data of Table 4 were combined with an adopted distance of $r = 2700$ pc and bolometric corrections (BC) defined by the relations of Alonso et al. (1999). For the Sun we adopted $M_{bol\odot} = 4.74$ mag (Bessell et al. 1998), $T_{\rm eff\odot} = 5700$ K and $\log g_{\odot} = 4.3$ dex.

It should be emphasized that for the nonmembers stars, adoption of the cluster parameters for distance, reddening, and metallicity will likely generate discordant results when compared to the spectroscopic parameters. For the six probable members, the temperature difference, in the sense (spectroscopic - photometric), is 52 ± 196 K, while the residuals in $\log g$ are 0.22 ± 0.33, consistent with the probable uncertainties in the estimates from the spectra, discussed above, and from the photometry. The modest offsets in temperature and gravity between the spectroscopic and photometric approaches are typical of such comparisons. Different methods are known to produce systematic offsets from each other, but there is no consensus on the source these offsets (e.g. Allende Prieto et al. 1999; Frebel et al. 2013).

The determination of the atmospheric parameters (Table 9) and the knowledge of the atomic parameters of the absorption lines enables us to obtain the chemical abundance by measuring the equivalent widths or by spectral synthesis. In the case of equivalent widths, MOOG uses atmospheric and atomic parameters, as well as equivalent widths measurements, to calculate the chemical abundance. For spectral synthesis, as input for MOOG we supply the atmospheric and atomic parameters and an estimate of the chemical abundance of the elements that influence the absorption line studied. Thereafter MOOG generates a synthetic spectrum which is compared with the observed spectrum, iterating until we find a chemical abundance that makes the synthetic spectra and observed identical.

Tables 11 and 12 show the chemical abundances of Na, Al, Fe-peak, alpha and s-process

elements in the notation [X/Fe] and its standard deviation. We analyzed a high-resolution FEROS solar spectrum to obtain the atmospheric parameters and solar abundance with the same methodology applied to red clump stars of Tombaugh 1. We found the following values for solar atmospheric parameters: $T_{\rm eff\odot} = 5700$ K, $\log g_{\odot} = 4.3$ dex and $\xi_{\odot} = 0.9$ $\rm km\,s^{-1}$. Pavlenko et al. (2012) found similar values of 5777 K, 4.44 dex and 0.8 $\rm km\,s^{-1}$ for the effective temperature, surface gravity and microturbulent velocity, respectively. In Table 10 we show our solar chemical abundances together with those given by Grevesse & Sauval (1998) and Asplund et al. (2009) for comparison. The adopted abundances for the elements analyzed in this work were normalized to our solar abundances. In the seventh row of Tables 11 and 12 we show the mean chemical abundance of Tombaugh 1 for each element with their respective standard deviations.

The approach to estimate the uncertainties in abundance consists in determining how the abundances for each element react to the errors associated with each atmospheric parameter, independent of the others. After that we combine quadratically all these errors and set this result as the total abundance uncertainty. These total uncertainties are given in the 5th column of Table 13 for star 769. We chose the star 769 to determine the abundance uncertainties for being one of the cluster giants that had the greatest number of elements with derived chemical abundance. The uncertainties for the aluminium weren't obtained for star 769 because their absorption lines are located in the spectral gaps, so we used star 663 to calculate the aluminium uncertainties. The uncertainties in abundance for the other stars generate similar values.

6. Results of Abundance Analysis

In this section we discuss the results of our chemical analysis via comparison with the chemical abundances of field giants stars and open clusters from the literature.

6.1. Metallicty and Iron-peak Elements

In Table 9 we show the metallicities obtained for our giants. The range of metallicity for the six stars classified as members of Tombaugh 1 is −0.16 to 0.10 dex, with the mean of -0.02 ± 0.05 dex. The spectroscopic values are consistent with photometric value of -0.10 ± 0.02. A weighted average of the two approaches gives a final [Fe/H] = −0.08 for Tombaugh 1. Comparison with past abundance estimates provides little insight given the large uncertainty in previous published estimates of this cluster parameter.

In Figures 11, 12 and 13 we show the abundance ratio of [X/Fe] versus metallicity for our sample of giants, for giants from Mishenina et al. (2006) and Luck & Heiter (2007), and also for the open clusters: NGC 6192, NGC 6404 and NGC 6583 (Magrini et al. 2010); NGC 3114 (Santrich et al. 2013); NGC 2527, NGC 2682, NGC 2482, NGC 2539, NGC 2335, NGC 2251 and NGC 2266 (Reddy et al. 2013); Trumpler 20 (Carraro et al. 2014b); NGC 4337 (Carraro et al. 2014d); NGC 4815 and NGC 6705 (Magrini et al. 2014); Cr 110, Cr 261, NGC 2477, NGC 2506 and NGC 5822 (Mishenina et al. 2015). For the s-process elements of Fig. 13, we added data of the open clusters Berkeley 25, Berkeley 73, Berkeley 75, Ruprecht 4, Ruprecht 7, NGC 6192, NGC 6404 and NGC 6583 from Mishenina et al. (2013).

From our chemical analysis of Tombaugh 1 we derive the following mean abundance ratios [X/Fe] for Cr and Ni: 0.10 ± 0.06 and -0.04 ± 0.02 dex, respectively. Our [Cr/Fe] and [Ni/Fe] of Tombaugh 1 are in good agreement with disk field giants and open clusters from literature as demonstrated in Figure 11.

6.2. Na, Al and alpha elements

Na is synthesized during hydrostatic carbon-burning in massive stars and also through the NeNa cycle during H-burning through the CNO-cycle in intermediate-mass and massive stars (Woosley & Weaver 1995; Denisenkov & Denisenkova 1990). The chemical analysis of Sodium must be performed taking into account NLTE effects, these effects being greater for higher equivalent widths and lower gravities (Gratton et al. 1999; Lind et al. 2011; Smiljanic 2012). In order to account for the NLTE effects in the Na abundances we used the corrections of Gratton et al. (1999). These corrections were typically smaller than 0.10 dex, with higher values for giants with lower $\log g$ (stars 784 and 1534). With this NLTE correction the range in the abundance ratio [Na/Fe] for the red clump stars of Tombaugh 1 goes from 0.38 to 0.05 dex, with a mean value of 0.17 $\pm$ 0.06. Star 1534, classified as a field giant, showed the strongest NLTE effects with a correction of 0.22 dex, mainly due to its low surface gravity ($\log g = 2.0$).

Chemical mixtures in the stellar interior can significantly modify the surface [Na/Fe] (e. g. Charbonnel & Lagarde 2010). Comparing Tombaugh 1 with the models of Charbonnel & Lagarde (2010), the mean cluster overabundance of [Na/Fe] = 0.17 among the giants is in excellent agreement with the values expected for models with thermohaline and rotation-induced mixing: [Na/Fe] = 0.18 for M = 2.0 $M_{\odot}$ and rotational velocities of 110 $\mathrm{km\,s^{-1}}$ on the ZAMS. The range of [Na/Fe] among the giants of Tombaugh 1 could be explained by a range of rotation velocities among the stars in ZAMS which produced the giants (Charbonnel & Lagarde 2010).

The production of Al, Mg, Si, Ca and Ti occurs mainly in massive stars whereas the production of the iron-peak elements is dominated by SN Type Ia (e. g. Woosley & Weaver 1995; Iwamoto et al. 1999). Thus, the chemical ratio of Al and alpha-elements with Fe can give us important information about the SNIa and SNII contributions to the galactic

components (bulge, disk and halo). The mean abundances of Mg, Si and Ca relative to Fe for Tombaugh 1 show essentially solar values of +0.03±0.05, +0.01±0.07 and +0.01±0.03, respectively. In the case of [Ti/Fe], we found for Tombaugh 1 a slightly overabundant value relative to the sun with a mean of +0.11±0.04 dex. Our values of [X/Fe] for alpha elements in Tombaugh 1 are consistent with the disk giants of Luck & Heiter (2007) and Mishenina et al. (2006) and also with open clusters with similar metallicity of literature (Figure 12). The decay of the [X/Fe] ratio to alpha elements with increasing of metallicity in the disk stars, as observed in the Figure 12, can be explained by the SNIa yields (Iwamoto et al. 1999), i.e. by high creation of Fe and low generation of alpha-elements. [Al/Fe] for Tombaugh 1 is similar to [Ti/Fe], with a mean of +0.15, in agreement with the chemical pattern of Al in the galactic disk (Figure 12).

6.3. Neutron-capture elements

The elements Y, Ba, Ce and Nd are formed mainly in the stellar interior by slow neutron-capture process (s-process) during the asymptotic giant branch (AGB) phase and are transported to the stellar surface by the third dredge-up (Busso et al. 1999). In Tombaugh 1, the light s-process element,Y, has a near solar [X/Fe] mean of +0.06 ± 0.04 dex while [X/Fe] for heavy s-process elements (Ba, Ce and Nd) shows an excess compared to the sun, with a mean of +0.35 ± 0.03 for Ba, +0.25 ± 0.06 for Ce, and +0.37 ± 0.05 for Nd. The difference between light and heavy s-process elements is an indicator of s-process efficiency (e. g. Luck & Bond 1981, 1991; Busso et al. 2001; Pereira et al. 2011), implying a high s-process efficiency for Tombaugh 1. Other open clusters exhibiting this same behavior include the Hyades (De Silva et al. 2006), Berkeley 18, Berkeley 21, Berkeley 22 and Berkeley 32 (Yong et al. 2012), Ruprecht 4, Ruprecht 7, NGC 6192 and NGC 6404 (Mishenina et al. 2013), among others. The s-process efficiency is an important

observational constraint to stellar evolutionary models (e.g. Busso et al. 2001) and is affected by metallicity, stellar mass and rotational velocity (e.g. Lugaro et al. 2003; Herwig et al. 2003).

Abundance measurements for s-process elements from the literature are highly inhomogeneous and difficult to compare with our results due to the use of different absorption lines, atomic parameters, and analysis methods (see. e.g., Yong et al. 2012 for a detailed discussion). Nevertheless, our s-process abundances for Tombaugh 1 agree with published s-process abundances for open clusters, as shown in Figure 13. Only our neodymium abundances show a slight overabundance with respect to open clusters and disk field giants from the literature.

6.4. The peculiar Tombaugh 1 field Cepheid XZ CMa

XZ CMa (star 806 in Table 4) is a short-period Cepheid (P=2^d.56, Caldwell & Coulson, 1987) situated within of coronal region of Tombaugh 1 but classified as not cluster member (see section 3.2). Three papers in the literature analyzed in detail the Cepheid XZ CMa (Turner, 1983; Diethelm, 1990; Yong et al. 2006). Turner (1983) and Diethelm (1990) conducted a photometric analysis of XZ CMa, while Yong et al. (2006) analyzed XZ CMa with a high-resolution spectroscopy. Turner (1983), via UBV photoelectric photometry, defined XZ CMa as unlikely member of Tombaugh 1 and found that XZ CMa probably has an unresolved blue companion which is aprox. 2.5 magnitudes fainter in V, due the phase of minimum in the U-V curve is shifted from the phase of minimum light by roughly 0.2 to 0.3 of the star's period. Subsequently, based in Walraven VBLUW photometric system, Diethelm (1990) derived the mean atmospheric parameters ($T_{\rm eff}$, $\log g$ and [Fe/H]) of XZ CMa, obtaining $T_{\rm eff}$=6000 K, $logg$=2.3 (dex) and [Fe/H]=-0.50 ± 0.10, with differences between our atmospheric parameters and Diethelm (1990) values of $\Delta T_{\rm eff}$=0 K, $\Delta logg$=0.4

(dex) and $\Delta[Fe/H]$=0.03 (dex).

Lastly, Yong et al. (2006) determined the atmospheric parameters and the chemical abundances of three alpha-elements (Si, Ca and TiII) to Cepheid XZ CMa, using same method but different line-list that used in this work. Our atmospheric parameters $T_{\rm eff}$, $\log g$ and ξ exhibit different values from those found by Yong et al. (2006), with differences of 750 K, 1.12 (dex) and 1.58 $\rm km\,s^{-1}$, respectively. However, we and Yong et al. (2006) obtained similiar values of metallicity to XZ CMa ($\Delta[Fe/H]$=0.04). Probably, the difference of $T_{\rm eff}$, $\log g$ and ξ displayed in this work and in Yong et al. (2006) is due to observation of Cepheid XZ CMa in distinct pulsation phase, which causes the determination of different values of atmospheric parameters ($T_{\rm eff}$, $\log g$ and ξ) and similar metallicity. Finally, in both studies an overabundance of alpha elements in XZ CMa was found, with mean of alpha elements in our analysis of [α/Fe]=0.13 and in Yong et al. (2006) of [α/Fe]=0.21, characteristic of Cepheid stars in the outer disk (e.g., see Fig 15 of Yong et al. 2006).

Our results show that Cepheid XZ CMa has a chemical pattern similar to that presented by disk field stars and open clusters (see Fig. 11 and 12). However, in Figure 13 we note that the Tombaugh 1 field star XZ CMa exhibits a high overabundance of Ba compared with field giants from literature. To demonstrate the high Ba abundance in this star, in Figure 14 we present the observed and synthetic spectra in the region around the absorption line of Ba II 5853 Å. Classical Cepheids, like XZ CMa, are not expected to present a high overabundance of s-process elements, as Ba, since such stars not evolved to AGB; e.g., cepheids FO Cas, EW Aur, EE Mon and FF Aur with similar metallicity of XZ CMa presents the ratio [Ba/Fe] of 0.17, 0.24, 0.03 and 0.13, respectively (Andrievsky et al., 2014). The chemical abundances of Ba in disk Cepheids is known to suffer from NLTE effects (Andrievsky et al. 2013; Andrievsky et al. 2014). However, the NLTE correction for Ba II line 5853 Å is not especially large, averaging around −0.1 dex (Andrievsky et al.

2013), does not having any significant effect in the high overabundance obtained for XZ CMa. We will discuss the case of this star in the final section.

7. Discussion and Conclusions

In this paper we have presented the first study of Tombaugh 1 using both high-resolution spectroscopy and precision $uvbyCa\mathrm{H}\beta$ photometry. Our results for the abundance ratios of elements from Na to Ni and the cluster fundamental parameters of distance and age tag this open cluster as an intermediate-age (0.95 Gyr) cluster belonging to the galactic thin disk. As such, it allows the addition of one more data point to the census of star clusters used to map the chemical history of the disk, falling within a galactocentric zone where there is universal agreement that a significant change in mean metallicity occurs among all classes of objects populating the thin disk. Where disagreement arises is in the exact form and location of the transition region. Does Tombaugh 1 lie along a uniform linear gradient extending from R_{GC} = 5 kpc to 20 kpc, or does the gradient change slope beyond the solar circle? If it changes, where does the transition occur and why? The growing evidence from studies of distant anticenter open clusters and Cepheids (e.g. Magrini et al. (2009); Lepine et al. (2011); Yong et al. (2012); Korotin et al. (2014), among others) is that the metallicity gradient beyond R_{GC} = 13 kpc is considerably flatter than that between 9 and 13 kpc (see Fig. 15).

In Figure 15 we show the radial metallicity gradient from Magrini et al. (2009) (blue points), with the addition of our spectroscopic results for Tombaugh 1 (red point) with [Fe/H] =$-0.02\pm$ 0.05 and R_{GC} = 10.46 kpc. If we use the lower photometric value of [Fe/H] =-0.10, R_{GC} would be reduced to 10.36 kpc, a negligible shift in distance on this scale. Also plotted are additional open clusters analyzed with high-resolution spectroscopy (green squares): IC 4725 and NGC 6087 (Gratton 2000); NGC 6603, NGC 2539, NGC

2447, IC 2714 and NGC 5822 (Santos et al. 2009); NGC 6192, NGC 6404 and NGC 6583 (Magrini et al. 2010); NGC 7160 (Monroe & Pilachowski 2010); Cr 110, NGC 2099, NGC 2420 and NGC 7789 (Pancino et al. 2010); Tombaugh 2 (Villanova et al. 2010); NGC 3114 (Santrich et al. 2013); NGC 4815 and NGC 6705 (Magrini et al. 2014); NGC 4337 (Carraro et al. 2014d); Trumpler 20 (Carraro et al. 2014b). The use of the spectroscopic value alone is tied to an apparent offset between the photometric abundance scale, for Strömgren photometry tied to high dispersion spectroscopy of F dwarfs, and the red giant high-dispersion spectroscopic scale, often distantly coupled to the sun. The issue is apparent in Fig. 15 where, inside R_{GC} = 9.8 kpc, no cluster has [Fe/H] below -0.1 and, more important, even ignoring the super-metal-rich outliers, the typical cluster [Fe/H] at all ages is +0.1. While a virtually identical pattern was found by Twarog et al. (1997), the lower limit and mean abundances from photometry and medium-resolution spectroscopy of cluster red giants were [Fe/H] $=-0.2$ and 0.0, respectively. Similar offsets between spectroscopic abundances of red giants and the photometry of F dwarfs have been found in NGC 3680 (Anthony-Twarog et al. 2009), NGC 5822 (Carraro et al. 2011), NGC 6819 (Anthony-Twarog et al. 2014), and NGC 752 (Twarog et al. 2015). In the cases of NGC 3680, NGC 6819, and NGC 752, high dispersion spectroscopic analysis of the F dwarfs agrees with the photometric abundances. If this offset to the spectroscopic scale applies to giants across all metallicities, the trend in Fig. 15 remains correct, even if the curve is shifted vertically by 0.1 dex.

We observe that Tombaugh 1 is consistent with the trend defined by Magrini et al. (2009) for the metallicity gradient, with Tombaugh 1 located in the inner disk ($R_{GC} \lesssim$ 12 kpc). The existence of an apparent transition zone ranging from R_{GC} = 10 to 12 kpc between an inner and outer disk lends support to the contention that metallicity evolution in these two regions occurs in different ways (Magrini et al. 2009; Lepine et al. 2011). According to Lepine et al. (2011), this behavior is due to a barrier created by a void in

the interstellar gas in the region of the corotation radius of the main spiral structure. This dynamical interaction produces an inward flow of the gas on the inside of the corotation zone of the Galaxy but an outward flow in the outer disk regions.

In recent years the abundances of the s-process elements in open clusters have become a target of intense study (e.g. D'Orazi et al. 2009, 2012; Jacobson et al. 2011; Maiorca et al. 2011; Jacobson & Friel 2013; Mishenina et al. 2013, 2015). This recent interest was sparked by the unexpected results of D'Orazi et al. (2009) for a sample of twenty open clusters. D'Orazi et al. (2009) found that [Ba/Fe] increases as cluster age decreases, contrary to the predictions of yields for Ba from AGB stars (e. g. Travaglio et al. 1999; Busso et al. 2001). Later work supplied confirmation for other s-process elements from unevolved stars in open clusters: Ba (Mishenina et al. 2013; Jacobson & Friel 2013), Ba and La (Jacobson et al. 2011), and Y, Zr, La, and Ce (Maiorca et al. 2011). However, Jacobson & Friel (2013) didn't find a trend for [X/Fe] for La and Zr versus age for their sample of 19 open clusters, which could indicate that the source of the s-process abundance trend with age doesn't affect all s-process elements equally. Among field stars, some s-process elements, Zr (Reddy et al. 2003) and Ba (Bensby et al. 2005), also show an increase in [X/Fe] with the decreasing age, while others, Y (Bensby et al. 2005), Ba and Ce (Reddy et al. 2003) do not.

In this context our photometric and spectroscopic analysis classifies Tombaugh 1 as intermediate age (0.95 Gyr), with an enrichment of heavy s-process elements (Ba with $+0.35 \pm 0.03$ dex, Ce with $+0.25 \pm 0.06$ dex and Nd with $+0.37 \pm 0.05$ dex) and solar values to Y ($+0.06 \pm 0.04$), indicating a high efficiency in the synthesis of the s-process elements. Some open clusters with similar ages show enrichment of the s-process elements similar to that found for Tombaugh 1, e.g. NGC 5822 (0.9 Gyr) (Carraro et al. 2011) and NGC 3680 (1.7 Gyr) (Anthony-Twarog et al. 2009) with [Ce/Fe] = 0.25 and [Ce/Fe] = 0.26, respectively (Maiorca et al. 2011).

The reason why open clusters younger than ∼1.5 Gyr (Maiorca et al. 2011) contain an overabundance of some s-process elements (mainly Ba) compared to the old open clusters still isn't understood. D'Orazi et al. (2009) and Maiorca et al. (2011) have proposed a scenario with models of extra-mixing phenomena with high efficiency in the production of the neutron source ^{13}C in stars with M $\leq$ 1.5M$_{\odot}$ (Busso et al. 2007; Nordhaus et al. 2008; Trippella et al. 2014; Nucci & Busso 2014). Very recently, Mishenina et al. (2015) suggested that the Ba overabundance in open clusters could be due to action from the intermediate neutron-capture process, or i-process (Cowan & Rose 1977). However, as Mishenina et al. (2015) pointed out, it remains difficult to know which open cluster stars would be the host of the i-process; low-metallicity stars are a more probable example of these hosts (Bertolli et al. 2013; Dardelet et al. 2015). Indeed, confirmation of the enrichment of s-process elements in young clusters requires the analysis of a large and homogeneous sample of young and old open clusters with well-determined s-process abundances.

The low number of open clusters with both reliable photometric and spectroscopic parameters, about 13.2% of the known open clusters as defined by the 2014 update of the Dias et al. (2002) catalog, is just one of the factors that hinder a definitive characterization of the galactic metallicity gradient, as well as its variation over time and azimuthally within the disk for individual elements. Studies of other poorly known open clusters like Tombaugh 1 using high-resolution spectroscopy and precision photometry to define reliably all of the key parameters that influence plots like Figs. 11, 12, 13 and 15 remain the key to forward progress in disentangling the complex system known as the galactic disk. The next step in this direction is being conducted by large surveys like Gaia-ESO mapping the chemistry of all the components of the Galaxy.

Finally, the overabundance of barium in Cepheid XZ CMa can be explained by an enhancement of s-process elements in the interstellar medium (ISM) which produced

XZ CMa or by mass transfer in a multiple-star system. Yong et al. (2006) found an enhancement of La for a Cepheid sample in the outer disk and suggested that asymptotic giant branch stars have contributed to the chemical evolution of the outer Galactic disk. XZ CMa is situated at the beginning of the outer disk (R_{GC}=13 Kpc, Yong et al. 2006), which makes XZ CMa one of the cepheid candidates rich in s-process elements formed by this ISM suggested by Yong et al. (2006).

In a binary system, like Ba and CH stars, the enrichment of Ba is a consequence of mass transfer through stellar winds or through Roche-lobe overflow from an AGB star (now the white dwarf) to a less evolved companion. Turner (1983) suggested the presence of an unresolved blue companion B star to the Cepheid XZ CMa. However, the enrichment of Ba indicates a white dwarf companion to XZ CMa. Thus, we suggest that XZ CMa can belong to a binary system with a white dwarf or a triple system comprising a white dwarf and a B star. About one-third of Galactic Cepheids are known to have companions, and about 44% of those have more than one companion (Evans et al. 2005). Recently, in the study of the occurrence of classical cepheids in binary systems, Neilson et al. (2015) pointed out that a fraction of binary systems may evolve to a system composed of a Cepheid with a white dwarf companion. Harris & Welch (1989) commented that due the occurrence of mass transfer in binary Cepheids an evolutionary connection between Ba stars and binary Cepheids would be possible. In addition, Gonzalez & Wallerstein (1996) found significant similarities between binaries Cepheids, and Ba and CH stars, as orbital parameters and mass range.

UV observations of XZ CMa can be used to confirm its binarity and reveal the nature of its companion (e.g. Evans 1992). In the case of a hot companion to XZ CMa like B main-sequence star suggested by Turner (1983), the presence of a strong Balmer line, Hϵ (3970.07 Å), in the Cepheid spectrum also can be interpreted as the signature of this blue

companion (Kovtyukh et al. 2015). Because of the wavelength coverage of our XZ CMa spectrum (4200 Åto 9000 Å) was not possible to perform this investigation. The discovery of binaries Cepheids is important because unresolved companions is one of the factors that contribute to the scatter around the ridge-line period-luminosity relationship (Szabados & Klagyivik, 2012). In particular, the detection of a Cepheid-white-dwarf binary will give important constraint regarding the most massive progenitors of white dwarfs (Landsman et al. 1996).

Extensive use was made of the WEBDA database maintained by E. Paunzen at the University of Vienna, Austria (http://www.univie.ac.at/webda). The filters used in the program were obtained by BJAT and BAT through NSF grant AST-0321247 to the University of Kansas. NSF support for this project was provided to BJAT and BAT through NSF grant AST-1211621. J.V. Sales Silva acknowledges the support provided by CNPq/Brazil Science without Borders program (project No. 249122/2013-8). C. Moni Bidin acknowledges support by the Fondo Nacional de Investigación Científica y Tecnológica (Fondecyt), project No. 1150060. E. Costa acknowledges support by the Fondo Nacional de Investigación Científica y Tecnológica (projecto No. 1110100, Fondecyt) and the Chilean Centro de Excelencia en Astrofísica y Tecnologías Afines (PFB 06).

Facilities: Magellan: Baade (IMACS), CTIO:1.0m (Y4KCam).

REFERENCES

Ahumada, J. E. & Lapasset, E. 1995, A&A, 109, 375

Allende Prieto, C., García López, R. J., Lambert, D. L., & Gustafsson, B. 1999, ApJ, 527, 879

Alonso, A., Arribas, S., Martínez-Roger, C. 1999, A&AS, 140, 261

Asplund, M., Grevesse, N., Sauval, A. J., & Scott, P. 2009, ARA&A, 47, 481

Andrievsky, S. M., Lépine, J. R. D., Korotin, S. A., et al. 2013, MNRAS, 428, 3252

Andrievsky, S. M., Luck, R. E., & Korotin, S. A. 2014, MNRAS, 437, 2106

Anthony-Twarog, B. J., Deliyannis, C. P., Twarog, B. A., Croxall, K. W., & Cummings, J. D. 2009, AJ, 138, 1171

Anthony-Twarog, B. J., Deliyannis, C. P., & Twarog, B. A. 2014, AJ, 148, 151

Bellazzini, M., Ibata, R., Monaco, L., et al. 2004, MNRAS, 354, 1263

Bensby, T., Feltzing, S., Lundström, I., & Ilyin, I. 2005, A&A, 433, 185

Bertolli, M. G., Herwig, F., Pignatari, M., & Kawano, T. 2013, arXiv:1310.4578

Bessell, M. S., Castelli, F., & Plez, B. 1998, A&A, 333, 231

Blackwell, D. E., Booth, A. J., Menon, S. L. R., & Petford, A. D. 1986, MNRAS, 220, 289

Busso, M., Gallino, R., & Wasserburg, G. J. 1999, ARA&A, 37, 239

Busso, M., Gallino, R., Lambert, D. L., Travaglio, C., & Smith, V. V. 2001, ApJ, 557, 802

Busso, M., Wasserburg, G. J., Nollett, K. M., & Calandra, A. 2007, ApJ, 671, 802

Caldwell, J. A. R., & Coulson, I. M. 1987, AJ, 93, 1090

Carraro, G. & Patat, F. 1995, MNRAS, 276, 563

Carraro, G., Moitinho, A., & V´zquez, R. A. 2008, MNRAS, 385, 1597

Carraro, G., Anthony-Twarog, B. J., Costa, E., Jones, B., & Twarog, B. A. 2011, AJ, 142, 127

Carraro, G., Giorgi, E. E., Costa, E., & Vázquez, R.A. 2014a, MNRAS, 441, L36

Carraro, G., Villanova, S., Monaco, L., et al. 2014b, A&A, 562, 39

Carraro, G., de Silva, G., Monaco, L., Milone, A. P., & Mateluna, R. 2014c, A&A, 566, 39

Carraro, G., Monaco, L., & Villanova, S. 2014, A&A, 568, A86

Carretta, E., Bragaglia, A., & Gratton, R. G. 2007, A&A, 473, 129

Castro, S., Rich, R. M., Grenon, M., Barbuy, B., McCarthy, J. K. 1997, AJ, 114, 376

Charbonnel, C., & Lagarde, N. 2010, A&A, 522, A10

Cowan, J. J., & Rose, W. K. 1977, ApJ, 212, 149

Crawford, D. L. 1975, AJ, 80, 955

Crawford, D. L. 1979, AJ, 84, 1858

Dardelet, L., Ritter, C., Prado, P., et al. 2015, arXiv:1505.05500

Depagne, E., Hill, V., Spite, M., et al. 2002, A&A, 390, 187

Denisenkov, P. A., & Denisenkova, S. N. 1990, Soviet Astronomy Letters, 16, 275

De Silva, G. M., Sneden, C., Paulson, D. B., et al. 2006, AJ, 131, 455

Dias, W. S., Alessi, B. S., Moitinho, A., & Lépine, J. R. D. 2002, A&A, 389, 871

Diethelm, R. 1990, A&A, 239, 186

D'Orazi, V., Magrini, L., Randich, S., et al. 2009, ApJ, 693, L31

D'Orazi, V., Biazzo, K., Desidera, S., et al. 2012, MNRAS, 423, 2789

Drake, J. J., & Smith, G. 1991, MNRAS, 250, 89

Dressler, A., Hare, T., Bigelow, B. C., & Osip, D. J. 2006, SPIE, 6269, 62690F

Edvardsson, B., Andersen, J., Gustafsson, B., et al. 1993, A&A, 275, 101

Evans, N. R. 1992, ApJ, 389, 657

Evans, N. R., Carpenter, K. G., Robinson, R., Kienzle, F., & Dekas, A. E. 2005, AJ, 130, 789

Frebel, A., Casey, A. R., Jacobson, H. R., & Yu, Q. 2013, ApJ, 769, 57

Gonzalez, G., & Wallerstein, G. 1996, MNRAS, 280, 515

Gratton, R. 2000, Stellar Clusters and Associations: Convection, Rotation, and Dynamos, 198, 225

Gratton, R. G., & Sneden, C. 1988, A&A, 204, 193

Gratton, R. G., Carretta, E., Eriksson, K., & Gustafsson, B. 1999, A&A, 350, 955

Grevesse, N. & Sauval, A. J. 1998, SSRv, 85, 161

Haffner, H. 1957, ZAp, 43, 89

Hauck, B. & Mermilliod, M. 1998, A&AS, 129, 431

Harris, H. C., & Welch, D. L. 1989, AJ, 98, 981

Herwig, F., Langer, N., & Lugaro, M. 2003, ApJ, 593, 1056

Iwamoto, K., Brachwitz, F., Nomoto, K., et al. 1999, ApJS, 125, 439

Jacobson, H. R., Friel, E. D., & Pilachowski, C. A. 2011, Bulletin of the American Astronomical Society, 43, #152.39

Jacobson, H. R., & Friel, E. D. 2013, AJ, 145, 107

Keeping, E. S. 1962, Introduction to Statistical Inference. London: Van Nostrand

Kharchenko, N. V., Piskunov, A. E., Schilbach, E., Rser, S., & Scholz, R.-D. 2013, A&A, 558, 53

Korotin, S. A., Andrievsky, S. M., Luck, R. E., et al. MNRAS, 444, 3301

Kovtyukh, V., Szabados, L., Chekhonadskikh, F., Lemasle, B., & Belik, S. 2015, MNRAS, 448, 3567

Kurucz, R. L. 1993, CD-ROM 13, Atlas9 Stellar Atmosphere Programs and 2 km/s Grid (Cambridge, MA: Smithsonian Astrophys. Obs)

Lambert, D. L., Heath, J. E., Lemke, M., & Drake, J. 1996, ApJS, 103, 183

Landsman, W., Simon, T., & Bergeron, P. 1996, PASP, 108, 250

Lépine, J. R. D., Cruz, P., Scarano, Jr., S., et al. 2011, MNRAS, 417, 698

Lind, K., Asplund, M., Barklem, P. S., & Belyaev, A. K. 2011, A&A, 528, A103

Luck, R. E., & Bond, H. E. 1981, ApJ, 244, 919

Luck, R. E., & Bond, H. E. 1991, ApJS, 77, 515

Luck, R. E., & Heiter, U. 2007, AJ, 133, 2464

Lugaro, M., Herwig, F., Lattanzio, J. C., Gallino, R., & Straniero, O. 2003, ApJ, 586, 1305

Magrini, L., Sestito, P., Randich, S., & Galli, D. 2009, A&A, 494, 95

Magrini, L., Randich, S., Zoccali, M., et al. 2010, A&A, 523, 11

Magrini, L., Randich, S., Romano, D., et al. 2014, A&A, 563, 44

Maiorca, E., Randich, S., Busso, M., Magrini, L., & Palmerini, S. 2011, ApJ, 736, 120

Majaess, D., Sturch, L., Moni Bidin, C., et al. 2013a, Ap&SS, 347, 61

Majaess, D., Carraro, G., Moni Bidin, C., et al. 2013b, A&A, 560, A22

Martin, W. C., Fuhr, J. R., Kelleher, D. E., et al. 2002, NIST Atomic Spectra Database (Version 2.0; Gaithersburg, MD: NIST)

McWilliam, A. & Rich, R. M. 1994, ApJS, 91, 749

Mishenina, T. V., Bienaymé, O., Gorbaneva, T. I., et al. 2006, A&A, 456, 1109

Mishenina, T., Korotin, S., Carraro, G., Kovtyukh, V. V., & Yegorova, I. A. 2013, MNRAS, 433, 1436

Mishenina, T., Pignatari, M., Carraro, G., et al. 2015, MNRAS, 446, 3651

Moni Bidin, C., Carraro, G., & Méndez, R. A. 2012, ApJ, 747, 101

Monroe, T. R., & Pilachowski, C. A. 2010, AJ, 140, 2109

Neilson, H. R., Schneider, F. R. N., Izzard, R. G., Evans, N. R., & Langer, N. 2015, A&A, 574, A2

Nissen, P. E. 1988, AJ, 199, 146

Nissen, P. E., Twarog, B. A., & Crawford, D. L. 1987, AJ, 93, 634

Nordhaus, J., Busso, M., Wasserburg, G. J., Blackman, E. G., & Palmerini, S. 2008, ApJ, 684, L29

Nucci, M. C., & Busso, M. 2014, ApJ, 787, 141

Olsen, E. H. 1983, A&AS, 54, 55

Olsen, E. H. 1988, A&A, 189, 173

Olsen, E. H. 1993, A&AS, 102, 89

Olsen, E. H. 1994, A&AS, 106, 257

Pancino, E., Carrera, R., Rossetti, E., & Gallart, C. 2010, A&A, 511, A56

Pavlenko, Y. V., Jenkins, J. S., Jones, H. R. A., Ivanyuk, O., & Pinfield, D. J. 2012, MNRAS, 422, 542

Pereira, C. B., Sales Silva, J. V., Chavero, C., et al. 2011, A&A, 533, A51

Piatti, A. E., Claría, J. J., & Ahumada, A. V. 2004, A&A, 421, 991

Preston, G. W., & Sneden, C. 2001, AJ, 122, 1545

Reddy, B. E., Bakker, E. J., & Hrivnak, B. J. 1999, ApJ, 524, 831

Reddy, B. E., Tomkin, J., Lambert, D.L., & Allende Prieto, C. 2003, MNRAS, 340, 304

Reddy, A. B. S., Giridhar, S., & Lambert, D. L. 2013, MNRAS, 431, 3338

Sales Silva, J. V., Peña Suárez, V. J., Katime Santrich, O. J., et al. 2014, AJ, 148, 83

Santos, N. C., Lovis, C., Pace, G., Melendez, J., & Naef, D. 2009, A&A, 493, 309

Santrich, O. J. K., Pereira, C. B., & Drake, N. A. 2013, A&A, 554, A2

Schmidt, E. G. 1984, ApJS, 55, 455

Smiljanic, R. 2012, MNRAS, 422, 1562

Sneden, C. A. 1973, Ph.D. Thesis, Univ. Texas

Snowden, M. S. 1975, PASP, 87, 721

Stetson, P. B. 1987, PASP, 99, 191

Szabados, L., & Klagyivik, P. 2012, Ap&SS, 341, 99

Tifft, W. G. 1959, ApJ, 129, 241

Tombaugh, C. W. 1938, PASP, 50, 171

Tombaugh, C. W. 1941, PASP, 53, 219

Travaglio, C., Galli, D., Gallino, R., et al. 1999, ApJ, 521, 691

Trippella, O., Busso, M., Maiorca, E., Käppeler, F., & Palmerini, S. 2014, ApJ, 787, 41

Turner, D. G. 1983, Journal of the Royal Astronomical Society of Canada, 77, 31

Twarog, B. A. & Anthony-Twarog, B. J. 1995, AJ, 109, 2828

Twarog, B. A., Ashman, K., & Anthony-Twarog, B. A. 1997, AJ, 114, 2556

Twarog, B. A., Anthony-Twarog, B. J., Deliyannis, C. P., & Thomas, D. 2015, AJ, in press

VandenBerg, D. A., Bergbusch, P. A., & Dowler, P. D. 2006, ApJS, 162, 375

van Dokkum, P. G. 2001, PASP, 113, 1420

Vásquez, R. A., May, J., Carraro, G., et al. 2008, ApJ, 672, 930

Villanova, S., Randich, S., Geisler, D., Carraro, G., & Costa, E. 2010, A&A, 509, A102

Wiese, W. L., Smith, M. W., & Miles, B. M. 1969, NSRDS-NBS, Washington, D.C.: US Department of Commerce, National Bureau of Standards, —c 1969,

Woosley, S. E., & Weaver, T. A. 1995, ApJS, 101, 181

Yong, D., Carney, B. W., Teixera de Almeida, M. L., & Pohl, B. L. 2006, AJ, 131, 2256

Yong, D., Carney, B. W., & Friel, E. D. 2012, AJ, 144, 95

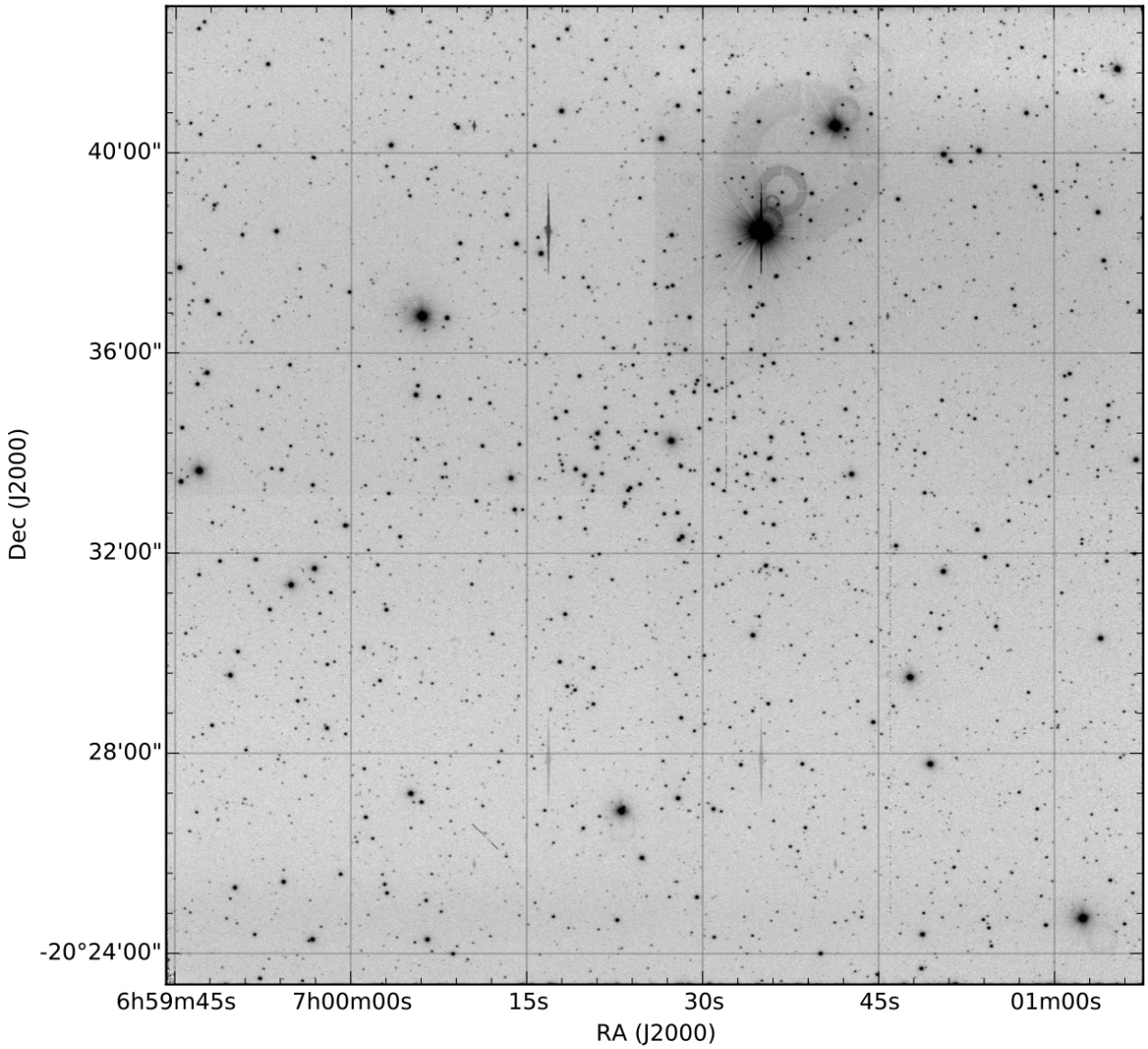

Fig. 1.— A 1200 sec exposure in the v filter. North is down and East to the right. The field is $20'$ on a side.

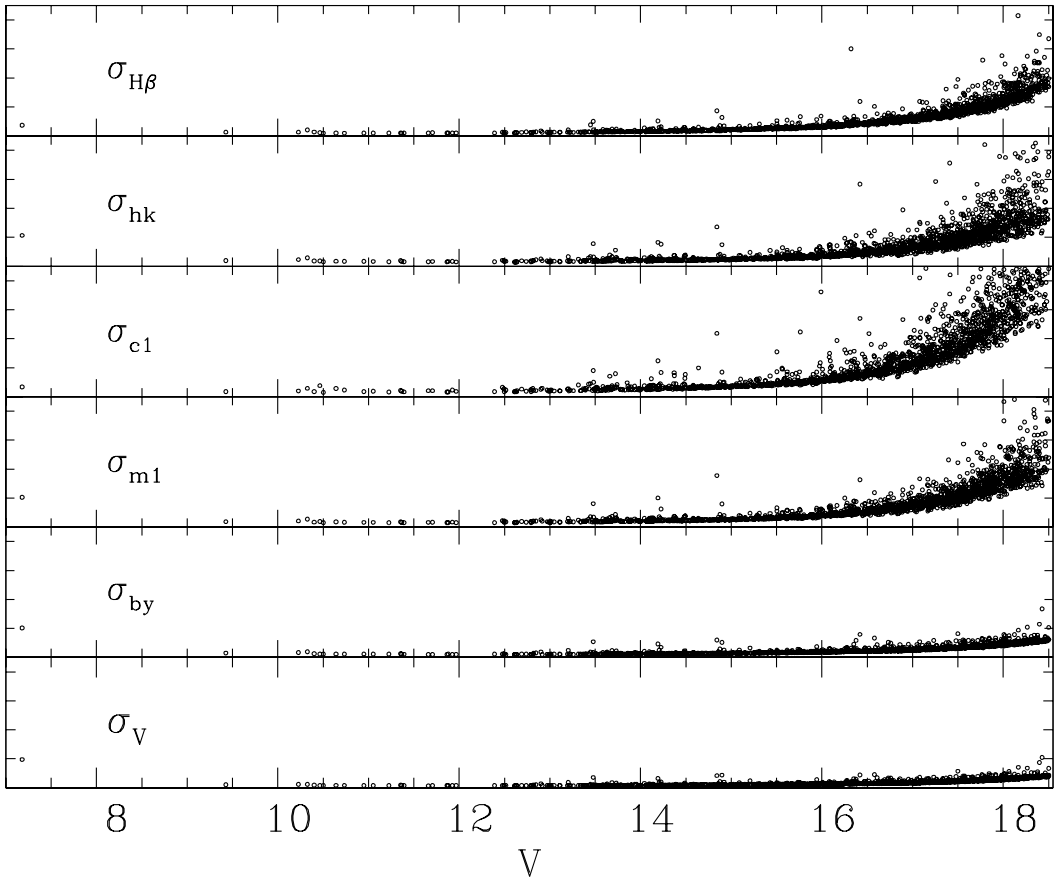

Fig. 2.— Trend of global photometric errors in magnitude and colors as a function of V magnitude. See text for details.

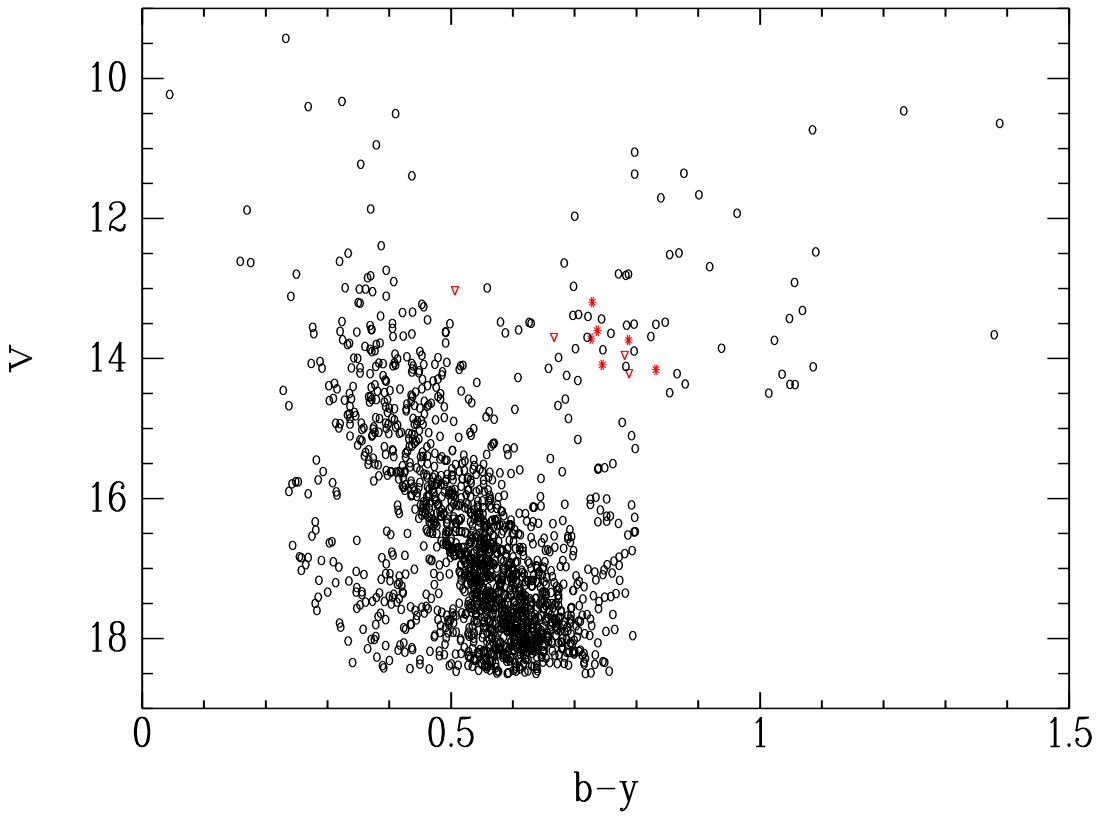

Fig. 3.— Color-magnitude diagram of Tombaugh 1. Red symbols identify the ten potential cluster stars observed with IMACS. Starred points are probable members, while open triangles are non-members. See text for details.

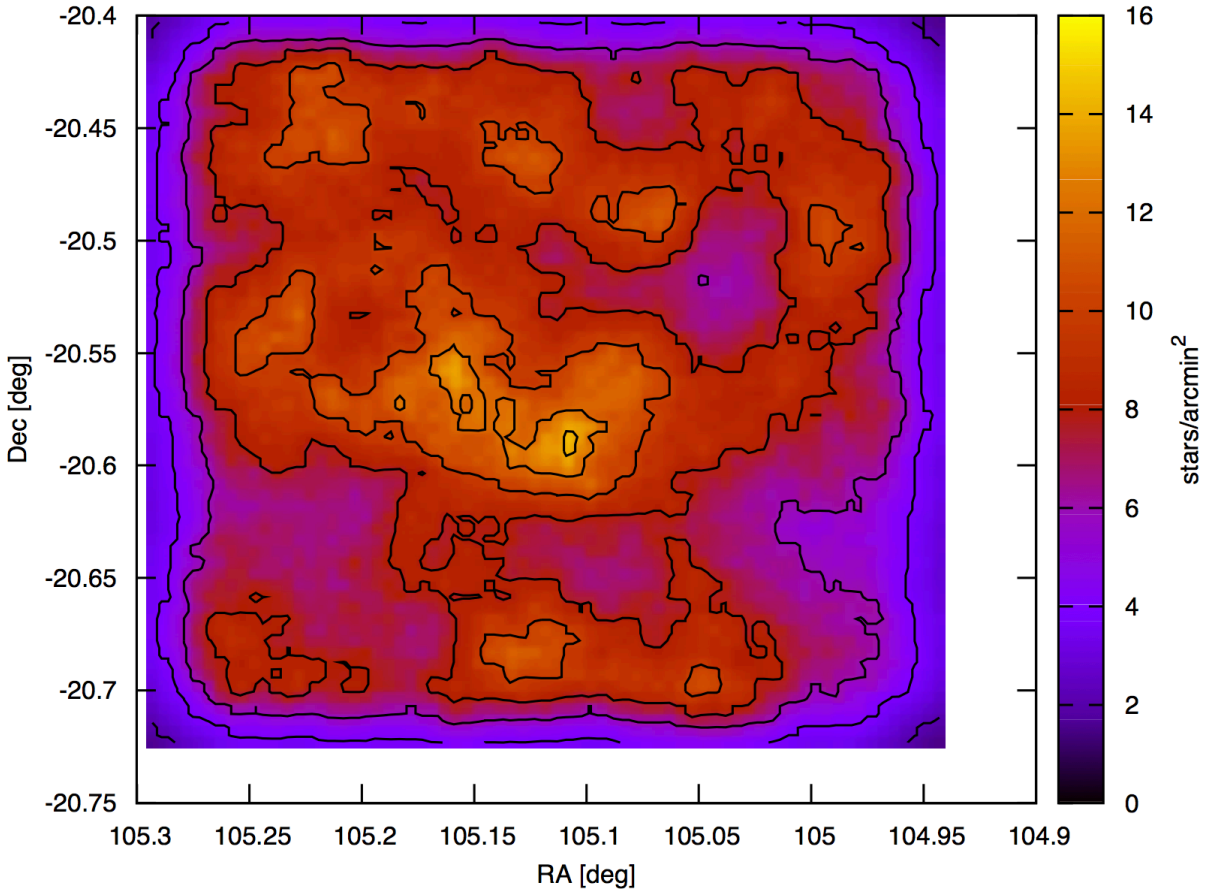

Fig. 4.— Density contour map for Tombaugh 1 field. North is up, East to the left, and the field corresponds to $20' \times 20'$ on the sky

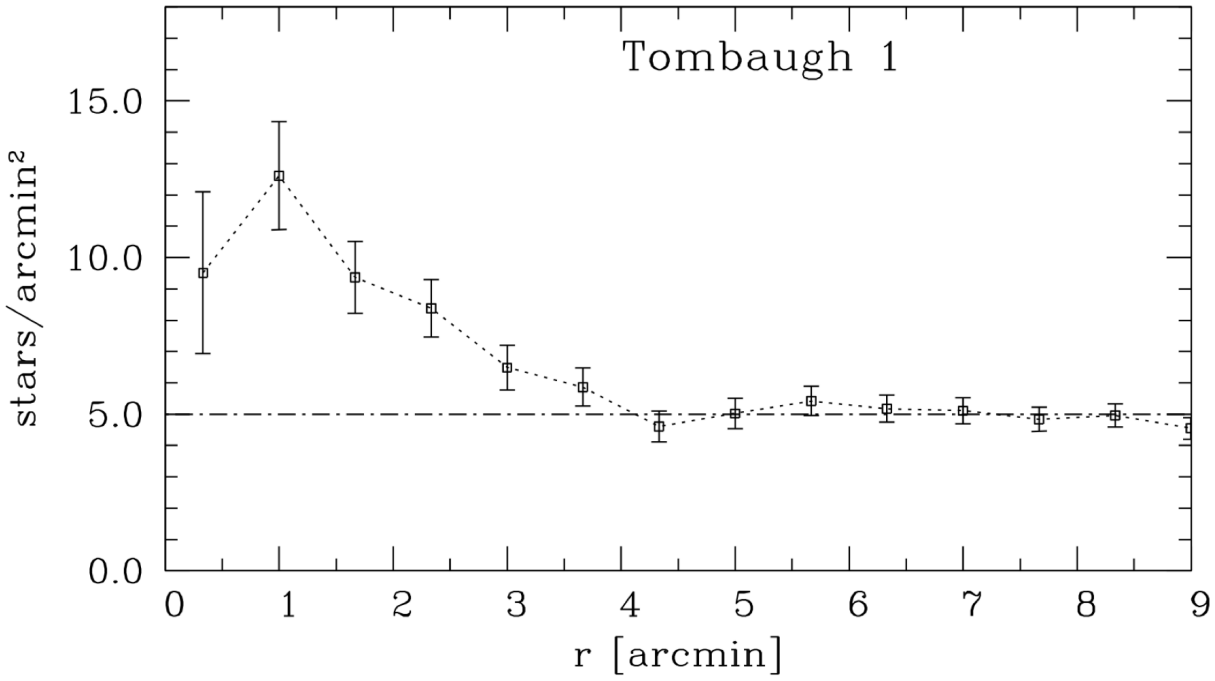

Fig. 5.— Radial surface density profile. To define concentric rings, we used the nominal cluster center.

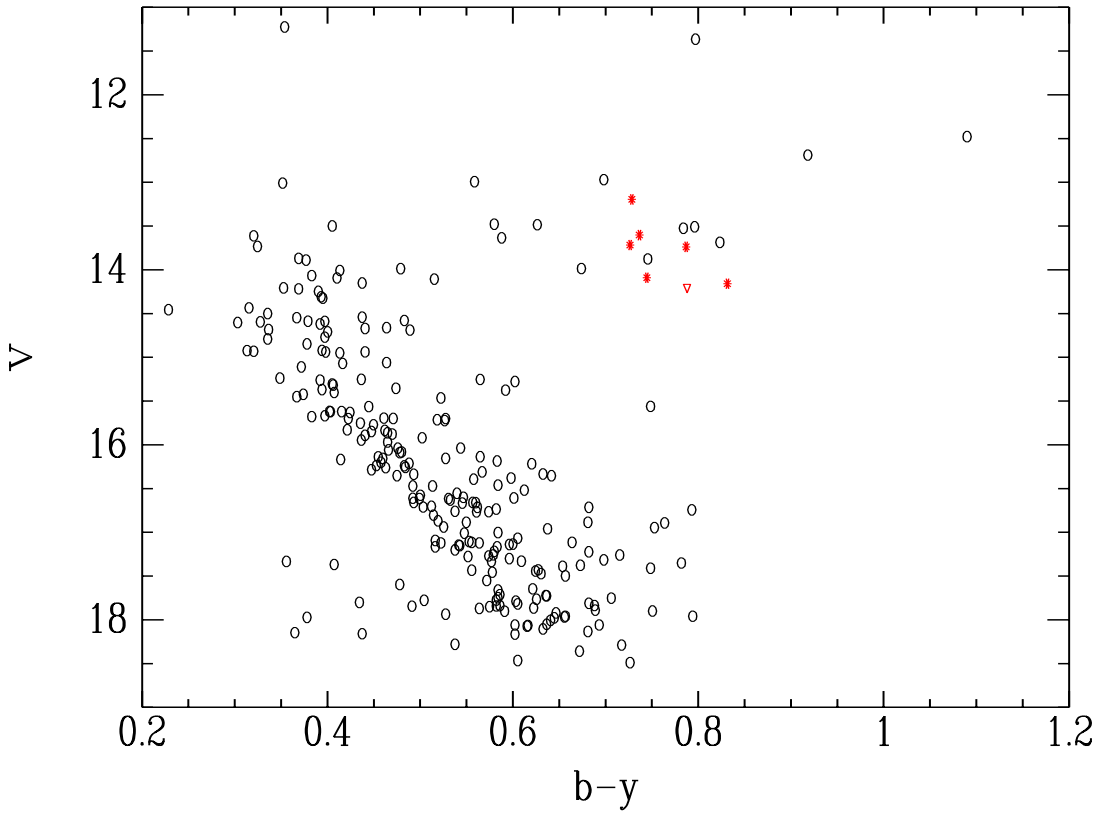

Fig. 6.— CMD of the cluster within 3.5′ of the cluster center. Symbols have the same meaning as in Fig. 3.

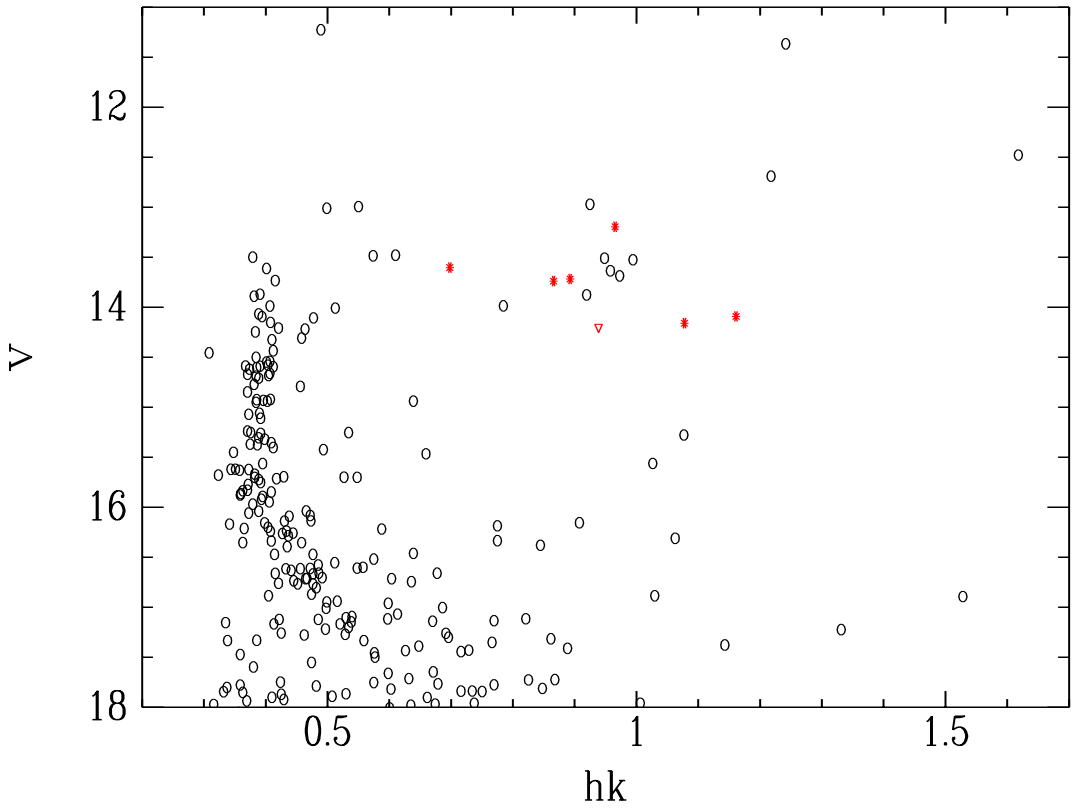

Fig. 7.— V, hk CMD of the cluster within $3.5'$ of the cluster center. Symbols have the same meaning as in Fig. 6.

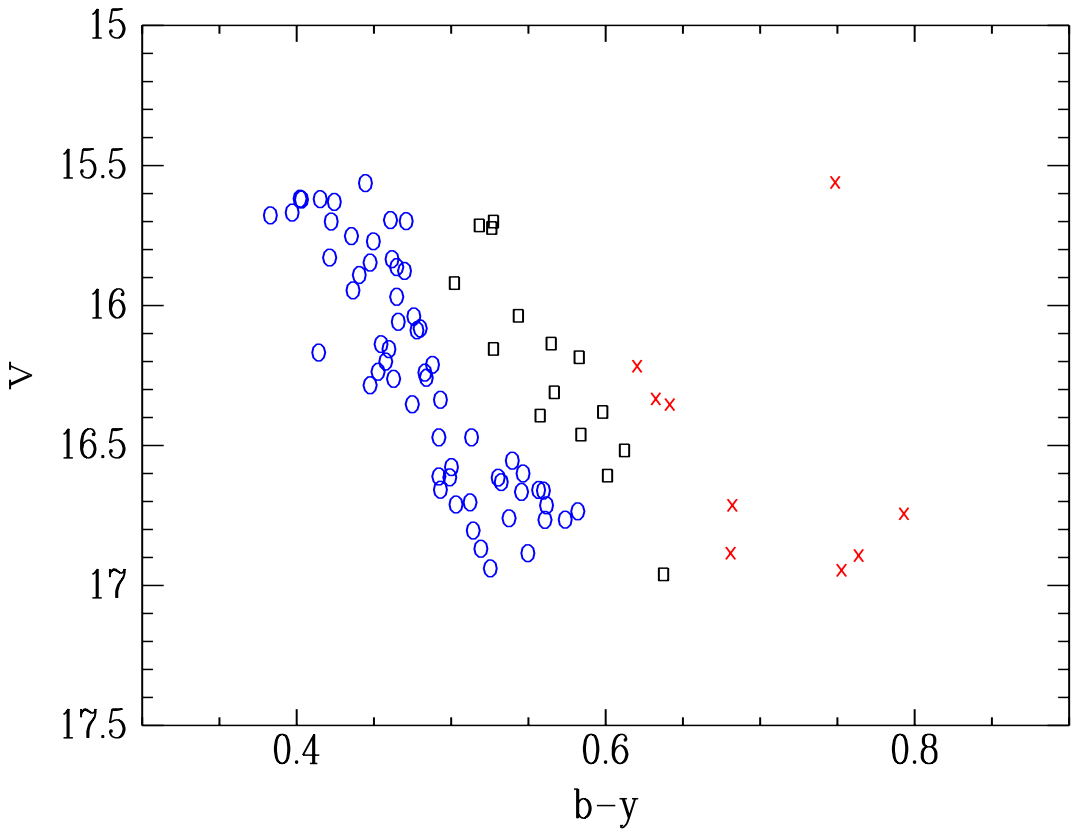

Fig. 8.— CMD of the cluster unevolved main sequence within 3.5′ of the cluster center. Blue open circles are probable single star members, black squares are potential binaries, and red crosses are likely nonmembers.

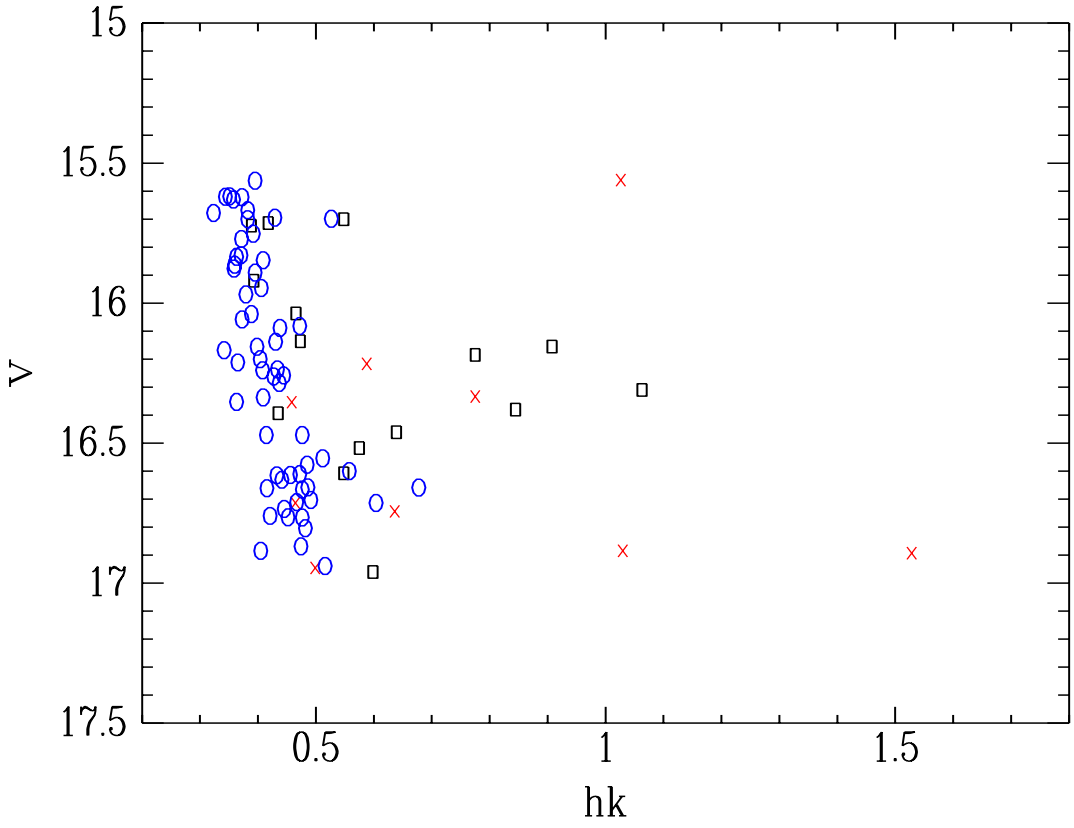

Fig. 9.— Same as Fig. 8 using *hk* as the temperature index.

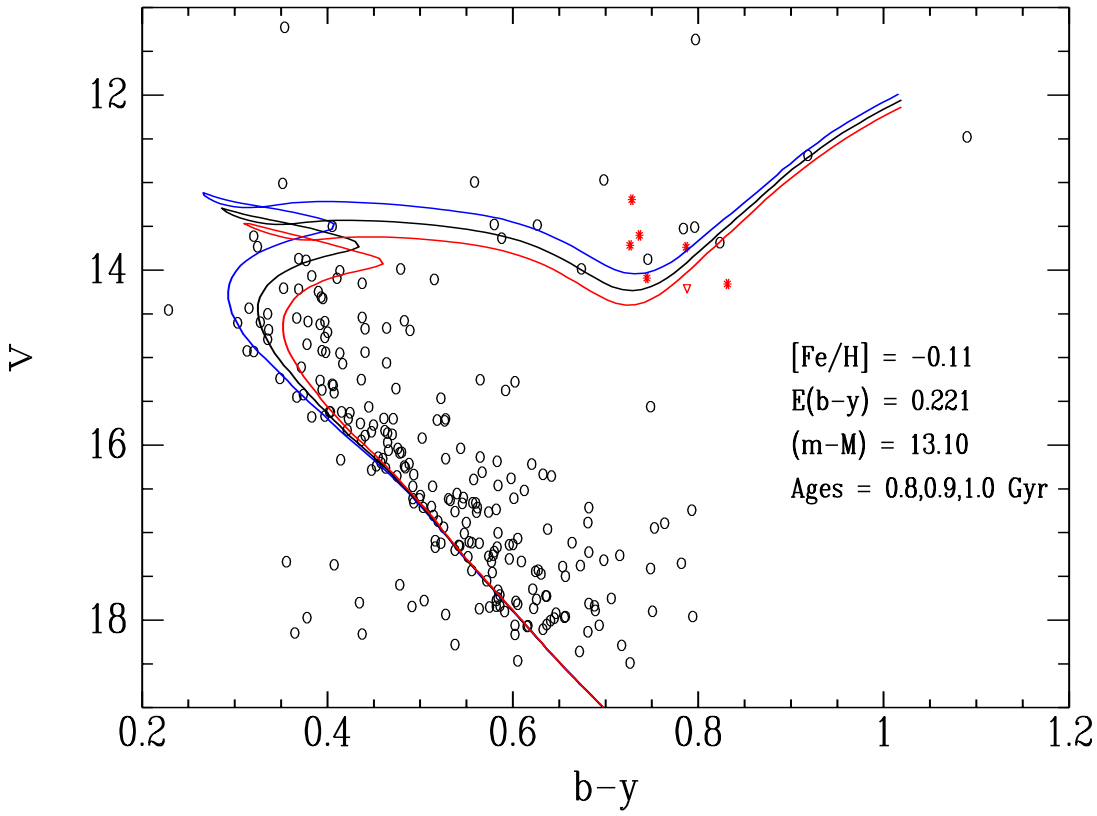

Fig. 10.— CMD of Fig. 6 superposed on the VR isochrones with [Fe/H] = −0.11, assuming $E(B-V) = 0.303$ and $(m-M) = 13.10$. The isochrones have ages of 0.8 Gyr (blue), 0.9 Gyr (black) and 1.0 Gyr (red).

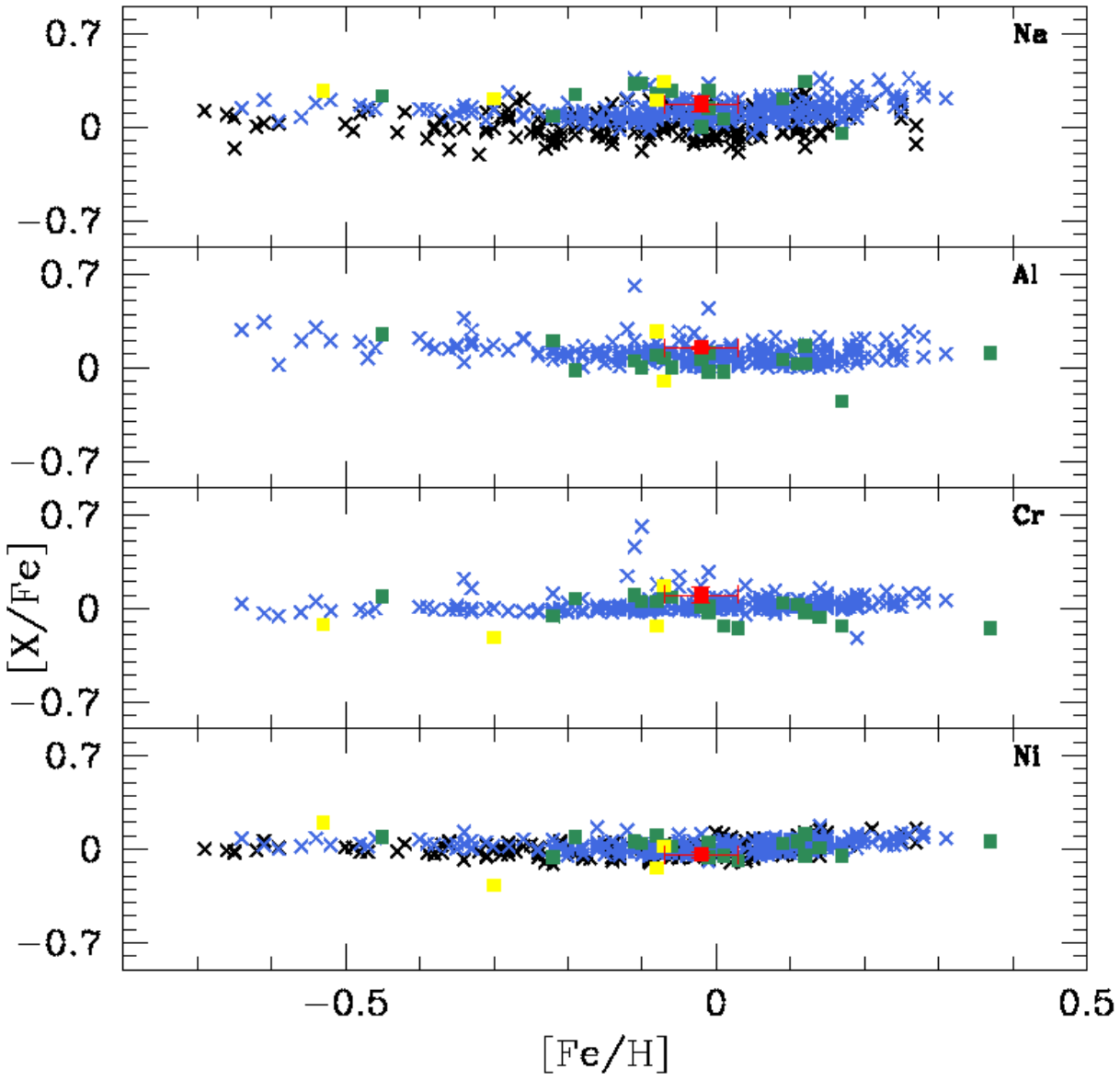

Fig. 11.— Abundance ratios [X/Fe] vs. [Fe/H]. Blue crosses: field giants of Luck & Heiter (2007); Black crosses: clump giants of Mishenina et al. (2006); Yellow squares: our sample of field giants stars; Red square: our mean abundances of Tombaugh 1; Green squares: open clusters from literature (NGC 6192, NGC 6404 and NGC 6583 of Magrini et al. 2010; NGC 3114 of Santrich et al. 2013; NGC 2527, NGC 2682, NGC 2482, NGC 2539, NGC 2335, NGC 2251 and NGC 2266 of Reddy et al. 2013; NGC 4337 of Carraro et al. 2014d; Trumpler 20 of Carraro et al. 2014b; NGC 4815 and NGC 6705 of Magrini et al. 2014; Cr 110, Cr 261, NGC 2477, NGC 2506 and NGC 5822 of Mishenina et al. 2015.

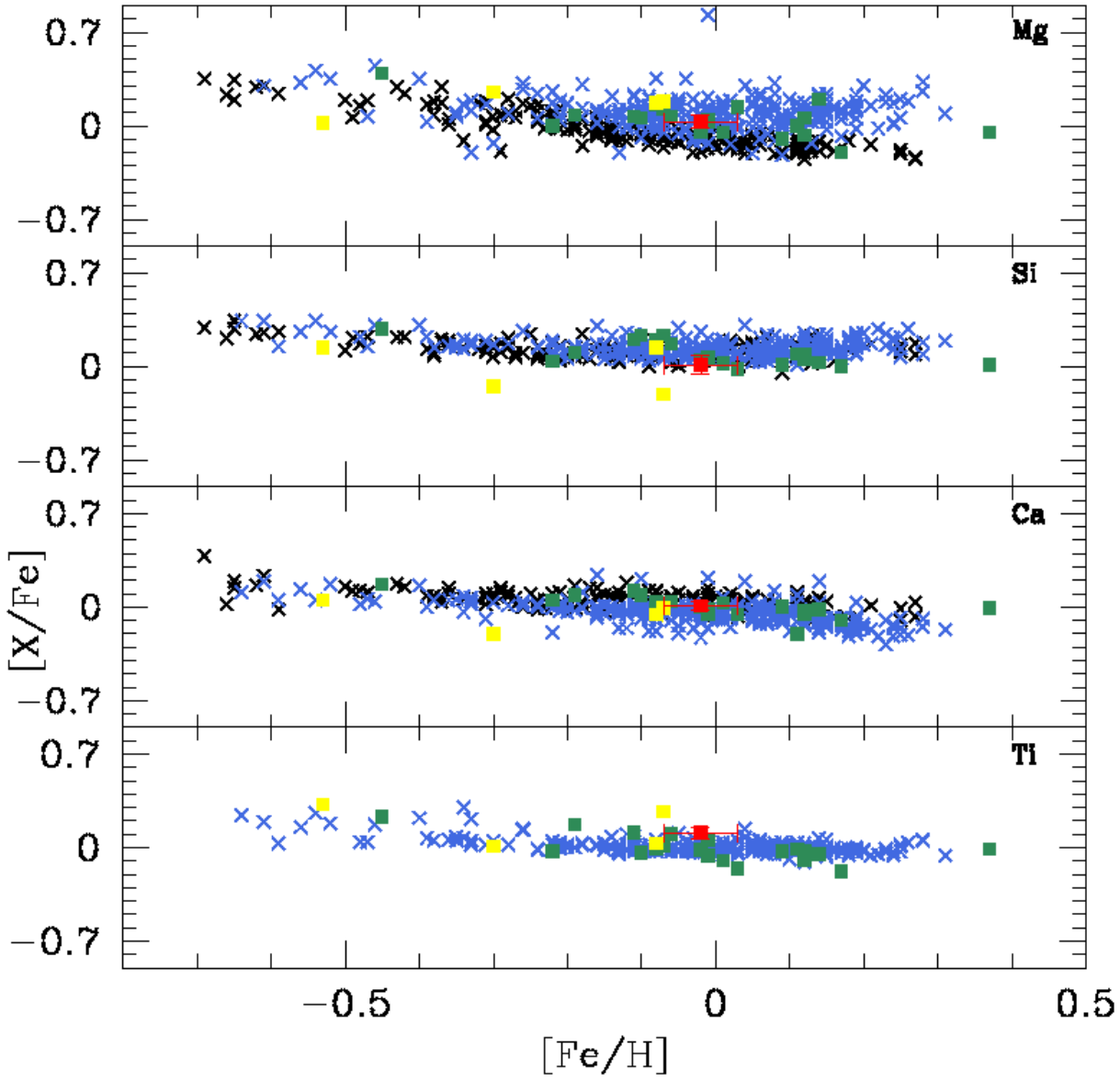

Fig. 12.— Abundance ratios [X/Fe] vs. [Fe/H]. Symbols have the same meaning as in Figure 11.

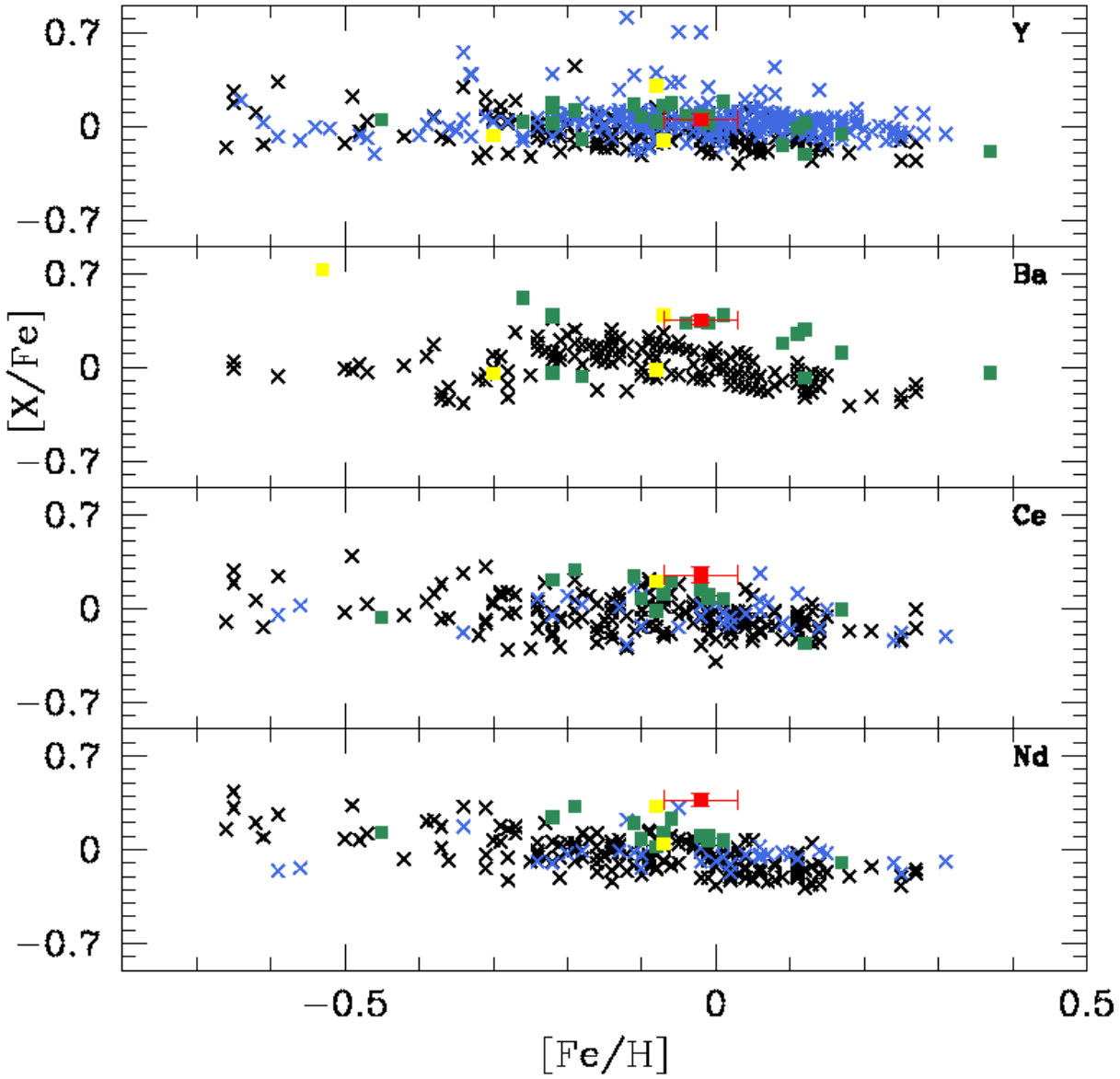

Fig. 13.— Abundance ratios [X/Fe] vs. [Fe/H]. Symbols have the same meaning as in Figure 11. In the Y and Ba panel, we added the results of Mishenina et al. (2013) of the open clusters Berkeley 25, Berkeley 73, Berkeley 75, Ruprecht 4, Ruprecht 7, NGC 6192, NGC 6404 and NGC 6583 (green squares). One field star of our sample (806) exhibits Ba enrichment.

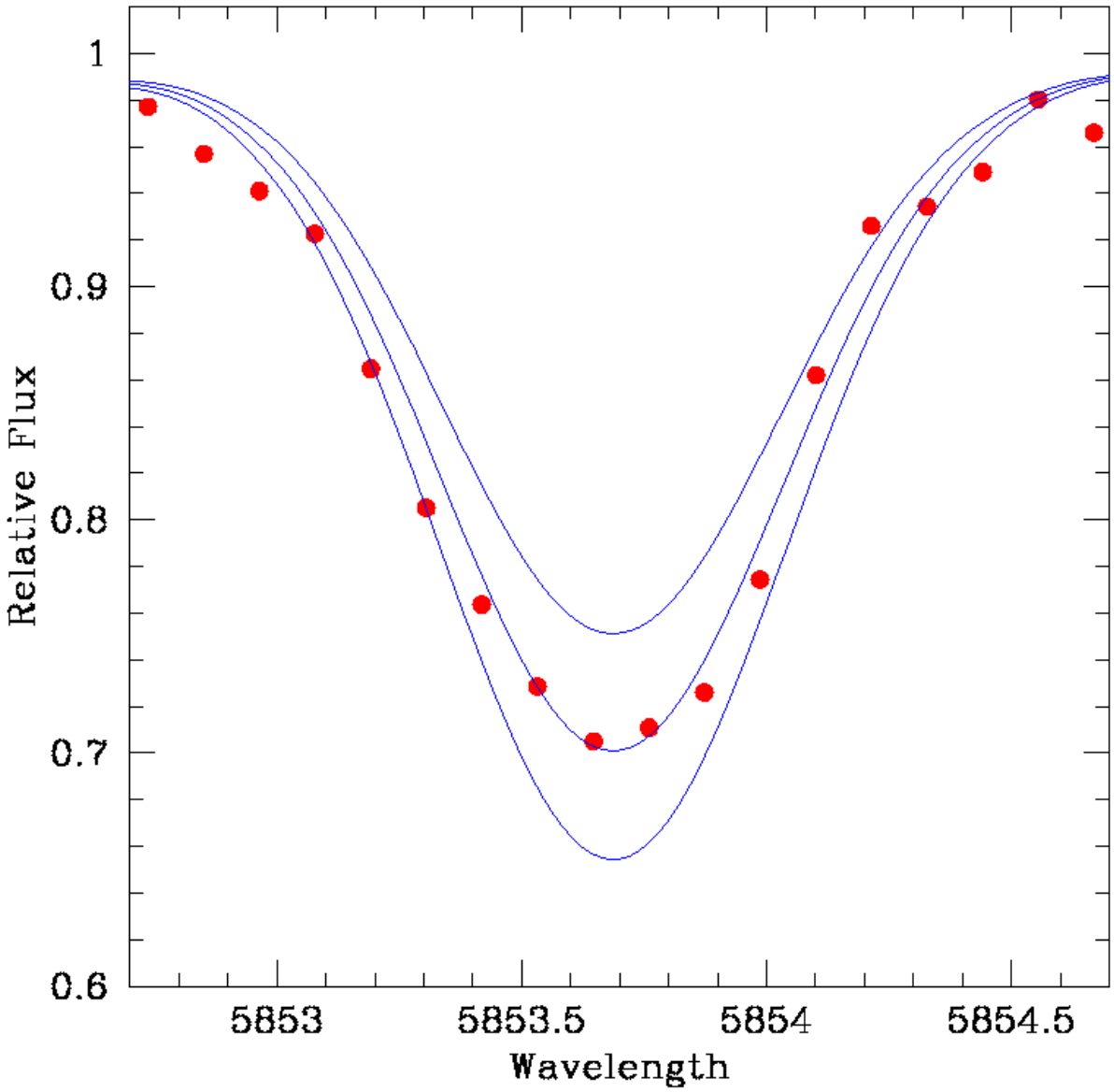

Fig. 14.— Observed (dotted red line) and synthetic spectra (solid blue lines) in the region of the Ba II line at 5853 Å for the field giant star 806. The synthetic spectra were calculated with the barium ratio abundances of [Ba/Fe]= 0.33, 0.73 and 1.13.

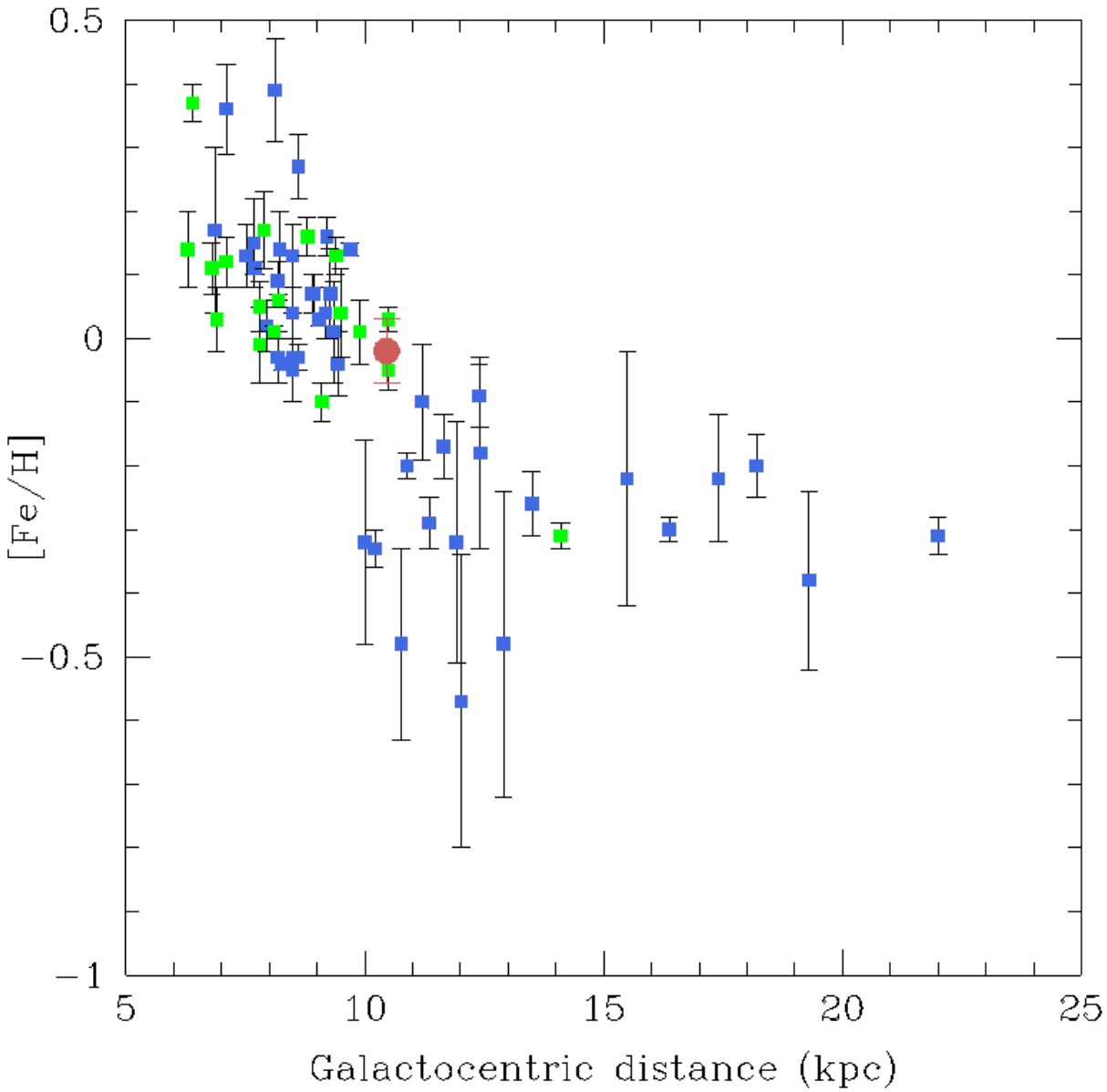

Fig. 15.— Radial metallicity gradient from Magrini et al. (2009, blue squares) with the addition of Tombaugh 1 (red circle) and additional open clusters analyzed with high-resolution spectroscopy (green squares). See text for details. $R_{GC\odot} = 8.5$ kpc.

Table 1: Strömgren photometric observations of Tombaugh 1

Date	Field	Filter	Exposures (sec)	airmass (X)
Dec 05, 2010	Tombaugh 1	y	60, 600	1.03
		b	60, 600	1.02
		$H\beta_{wide}$	60, 600	1.01−1.02
		Ca	120, 1200	1.01
		$H\beta_{narrow}$	120,1200	1.02
Dec 06, 2010	Tombaugh 1	y	2x60, 900	1.03
		b	2x60,900	1.02
		v	60, 900	1.01−1.03
		Ca	120,1500	1.04-1.08
Dec 07 , 2010	Tombaugh 1	u	10, 300	1.02
		b	10, 60	1.01
		v	10, 100	1.01
		Ca	10, 200	1.01
		$H\beta_{wide}$	10, 60	1.01−1.01
		$H\beta_{narrow}$	10, 200	1.02
Dec 08, 2010	Tombaugh 1	u	2x20, 200 2000	1.02−1.03
		v	20, 90, 900	1.01−1.03
		$H\beta_{narrow}$	20, 150, 1500	1.05
Dec 09, 2010	Tombaugh 1	y	10, 60, 120, 600	1.46−1.51
		b	60,180,900	1.35−1.39
		v	100, 200, 1200	1.25−1.28
		Ca	100, 300,1800	1.04−1.05
		$H\beta_{wide}$	100, 200, 1200	1.16−1.18
		$H\beta_{narrow}$	10, 300, 1800	1.09−1.11
Dec 09, 2010	Tombaugh 1	y	60, 600	1.47−1.49
		b	180, 900	1.38−1.40
		v	200, 900	1.30
		Ca	300, 1500	1.07−1.08
		$H\beta_{wide}$	200, 900	1.30
		$H\beta_{narrow}$	300, 1500	1.13−1.14
		u	400, 1800	1.03−1.04

Table 2: Calibration Equations Summary

Index	slope	color term	Std. deviation
V	1.00	0.05	0.010
$b-y$	1.01	—	0.002
hk	1.07	—	0.009
Hβ	1.18	—	0.015
m_1	0.92	-0.075	0.025
c_1	1.06	—	0.021

Table 3: Excerpt of the photometric catalog of Tombaugh 1.

$\alpha(2000)$	$\delta(2000)$	V	$b-y$	hk	$H\beta$	m_1	c_1	σ_V	σ_{by}	σ_{m1}	σ_{c1}	σ_{hk}	σ_β
105.1726	−20.6754	7.179	0.826	1.377	2.532	0.453	0.187	0.0195	0.0204	0.0205	0.0067	0.0213	0.0074
105.0252	−20.6121	9.426	0.232	0.326	2.769	0.119	0.793	0.0021	0.0030	0.0037	0.0035	0.0040	0.0026
105.2605	−20.4113	10.227	0.044	0.234	2.915	0.145	1.012	0.0023	0.0034	0.0042	0.0039	0.0046	0.0026
105.1471	−20.6414	10.326	0.323	0.550	2.673	0.158	0.406	0.0023	0.0039	0.0055	0.0057	0.0058	0.0042
105.0961	−20.4473	10.400	0.268	0.473	2.716	0.209	0.613	0.0018	0.0026	0.0034	0.0034	0.0037	0.0027
105.2796	−20.5640	10.463	1.232	1.976	2.574	0.661	-0.319	0.0016	0.0023	0.0038	0.0076	0.0037	0.0022
104.9458	−20.5607	10.502	0.410	0.585	2.582	0.167	0.251	0.0016	0.0023	0.0030	0.0030	0.0032	0.0019
105.0569	−20.5582	10.641	1.387	1.216	2.754	0.050	0.134	0.0017	0.0024	0.0035	0.0056	0.0035	0.0020
105.0750	−20.6804	10.733	1.084	1.836	2.550	0.639	-0.147	0.0017	0.0023	0.0033	0.0046	0.0034	0.0019
105.1990	−20.4917	10.947	0.379	0.568	2.620	0.134	0.411	0.0016	0.0024	0.0032	0.0035	0.0034	0.0020
105.0211	−20.4531	11.051	0.797	1.338	2.550	0.471	0.199	0.0017	0.0023	0.0032	0.0037	0.0033	0.0020

Table 4: Potential cluster stars observed with IMACS in the field of Tombaugh 1.

ID	RA(2000.0)	DEC(2000.0)	V	$b-y$	$V-I$	RV_1	RV_2	$\langle RV \rangle$	vsini	S/N
	hh:mm:ss	dd:mm:ss	mag	mag	mag	(km s^{-1})	(km s^{-1})	(km s^{-1})	(km s^{-1})	
395	07 : 00 : 05.7	−20 : 35 : 20.5	13.72	0.73	1.19	81.6±1.8	82.7±2.4	82.1±0.7	<2.7	100
663	07 : 00 : 18.7	−20 : 31 : 31.0	14.09	0.75	1.19	79.9±2.6	79.8±2.8	79.8±0.1	<2.7	60
769	07 : 00 : 23.4	−20 : 32 : 59.2	13.20	0.73	1.20	81.6±1.4	81.5±1.5	81.5±0.0	<2.7	110
784	07 : 00 : 24.1	−20 : 35 : 45.1	14.20	0.79	1.26	99.0±2.2	98.8±1.3	98.9±0.1	5.6±0.9	55
806[a]	07 : 00 : 24.8	−20 : 25 : 54.1	13.01	0.51	1.12	100.0±2.1	99.0±3.8	99.5±0.6	—	95
1110	07 : 00 : 36.1	−20 : 35 : 47.1	13.60	0.74	1.27	84.0±2.4	84.7±2.4	84.3±0.5	6.1±0.5	100
1118	07 : 00 : 36.5	−20 : 38 : 57.4	13.74	0.79	1.32	82.2±2.3	81.1±2.9	81.7±0.7	<2.7	74
1349	07 : 00 : 46.3	−20 : 28 : 55.7	14.16	0.83	1.32	77.2±3.8	76.5±3.3	76.8±0.5	5.1±0.4	44
1534	07 : 00 : 54.5	−20 : 24 : 30.0	13.94	0.78	1.31	93.8±3.6	91.8±4.6	92.8±1.3	—	50
1616	07 : 00 : 58.1	−20 : 33 : 24.6	13.68	0.67	1.11	42.7±2.4	44.8±2.9	43.7±1.3	4.2±0.4	100

Notes. The columns inform, from left to right: star identification, right ascension, declination, V and b-y from this paper, and V-I from Carraro & Patat (1995), two epoch heliocentric radial velocities (RV_1 and RV_2) and their mean values ($\langle RV \rangle$), projected rotational velocities (vsini) and spectral signal-to-noise at 6000 Å. (a) The classical Cepheid XZ CMa.

Table 5: Observed Fe I and Fe II lines.

				Equivalent Widths (mÅ)				
				Star				
Element	λ (Å)	χ(eV)	log gf	769	806	1110	1118	395
Fe I	5159.06	4.28	−0.650	—	—	—	83	110
	5162.27	4.18	0.079	158	148	—	—	153
	5198.71	2.22	−2.140	132	140	107	—	125
	5242.49	3.63	−0.970	105	—	—	—	111
	5250.21	0.12	−4.920	—	—	—	—	136
	5288.52	3.69	−1.510	—	37	63	79	78
	5307.36	1.61	−2.970	—	94	111	125	133
	5315.05	4.37	−1.400	—	—	59	—	51
	5321.11	4.43	−1.190	60	—	—	—	—
	5322.04	2.28	−2.840	—	31	78	—	103
	5364.87	4.45	0.230	136	—	126	150	143
	5367.47	4.42	0.439	141	—	131	135	142
	5373.71	4.47	−0.710	85	—	70	77	—
	5410.91	4.47	0.400	—	—	140	—	—
	5417.03	4.42	−1.530	53	—	33	39	61
	5441.34	4.31	−1.580	47	18	46	58	65
	5522.45	4.21	−1.400	67	—	47	58	60
	5531.98	4.91	−1.460	37	—	31	29	—
	5554.90	4.55	−0.380	—	73	—	—	—
	5560.21	4.43	−1.040	70	—	63	64	72
	5567.39	2.61	−2.560	—	—	76	—	110
	5576.09	3.43	−0.850	135	—	—	—	—
	5633.95	4.99	−0.120	96	68	—	81	—
	5635.82	4.26	−1.740	58	—	—	47	56
	5638.26	4.22	−0.720	—	—	—	—	96
	5691.50	4.30	−1.370	—	23	66	54	79
	5705.47	4.30	−1.360	64	—	68	57	—
	5731.76	4.26	−1.150	—	—	—	—	76
	5806.73	4.61	−0.900	73	—	—	65	62
	5852.22	4.55	−1.180	62	—	48	—	60
	5883.82	3.96	−1.210	90	—	69	—	—
	5934.65	3.93	−1.020	97	—	—	—	92
	6020.17	4.61	−0.210	—	101	—	—	—
	6024.06	4.55	−0.060	—	—	109	119	126
	6027.05	4.08	−1.090	103	44	80	87	95
	6056.01	4.73	−0.400	93	—	78	81	86
	6065.48	2.61	−1.530	157	—	125	154	156

Table 5, continued.

				Equivalent Widths (mÅ)				
				Star				
Element	λ (Å)	χ(eV)	log gf	769	806	1110	1118	395
Fe I	6079.01	4.65	−0.970	—	—	—	71	—
	6096.66	3.98	−1.780	56	—	50	49	62
	6120.25	0.91	−5.950	—	—	24	—	—
	6151.62	2.18	−3.290	92	—	75	90	92
	6157.73	4.08	−1.110	98	36	89	94	89
	6165.36	4.14	−1.470	59	—	59	73	59
	6170.51	4.79	−0.380	—	36	—	—	—
	6173.34	2.22	−2.880	107	39	92	112	122
	6187.99	3.94	−1.570	73	—	60	72	80
	6200.31	2.60	−2.440	118	—	—	107	103
	6213.43	2.22	−2.480	123	—	—	—	—
	6265.13	2.18	−2.550	128	95	—	132	135
	6311.50	2.83	−3.230	—	—	—	57	—
	6322.69	2.59	−2.430	—	—	88	—	106
	6380.74	4.19	−1.320	87	—	65	86	70
	6392.54	2.28	−4.030	—	—	29	—	—
	6411.65	3.65	−0.660	142	150	125	138	—
	6421.35	2.28	−2.010	—	152	135	153	150
	6430.85	2.18	−2.010	155	—	126	155	159
	6436.41	4.19	−2.460	25	—	—	—	—
	6469.19	4.83	−0.620	85	29	74	79	71
	6593.87	2.44	−2.420	124	—	—	117	129
	6597.56	4.79	−0.920	71	—	—	55	57
	6608.03	2.28	−4.030	48	—	28	39	37
	6646.93	2.61	−3.990	45	—	—	—	30
	6653.85	4.14	−2.520	26	—	—	—	—
	6703.57	2.76	−3.160	81	—	—	64	59
	6739.52	1.56	−4.950	37	—	—	41	—
	6750.15	2.42	−2.620	106	—	95	—	102
	6752.71	4.64	−1.200	69	—	48	59	59
	6806.85	2.73	−3.210	63	—	63	—	64
	6810.26	4.61	−0.990	58	—	—	73	74
	6820.37	4.64	−1.170	62	—	—	58	72
	6851.64	1.61	−5.320	—	—	—	—	24
	6858.15	4.61	−0.930	77	—	68	63	—
	7130.92	4.22	−0.700	115	85	—	—	103
	7132.99	4.08	−1.610	63	25	49	—	65
Fe II	5132.66	2.81	-4.000	—	—	44	—	—
	5425.25	3.20	−3.210	—	—	—	63	67

Table 5, continued.

				Equivalent Widths (mÅ)				
				Star				
Element	λ (Å)	χ(eV)	log gf	769	806	1110	1118	395
Fe II	5991.37	3.15	−3.560	—	—	43	—	—
	6084.10	3.20	−3.800	—	—	35	45	—
	6149.25	3.89	−2.720	—	—	43	—	60
	6247.55	3.89	−2.340	81	139	—	74	82
	6416.92	3.89	−2.680	54	96	49	—	52
	6432.68	2.89	−3.580	61	—	50	—	63

Table 6: Observed Fe I and Fe II lines.

				Equivalent Widths (mÅ)				
				Star				
Element	λ (Å)	χ(eV)	log gf	1534	1616	1349	784	663
Fe I	5159.06	4.28	−0.650	—	98	106	109	—
	5253.03	2.28	−3.790	—	—	—	—	91
	5288.52	3.69	−1.510	—	—	—	93	116
	5307.36	1.61	−2.970	—	109	147	148	—
	5315.05	4.37	−1.400	—	—	—	—	70
	5321.11	4.43	−1.190	—	—	—	—	98
	5322.04	2.28	−2.840	121	—	—	—	—
	5364.87	4.45	0.230	158	—	148	154	—
	5367.47	4.42	0.439	157	—	—	—	—
	5373.71	4.47	−0.710	116	—	113	89	116
	5417.03	4.42	−1.530	53	52	60	61	80
	5441.34	4.31	−1.580	44	40	57	—	—
	5522.45	4.21	−1.400	—	—	68	71	92
	5554.90	4.55	−0.380	—	103	122	—	—
	5560.21	4.43	−1.040	—	—	104	—	—
	5567.39	2.61	−2.560	122	—	—	—	155
	5576.09	3.43	−0.850	—	—	—	154	—
	5624.02	4.39	−1.330	—	—	—	76	103
	5633.95	4.99	−0.120	—	85	103	—	—
	5635.82	4.26	−1.740	—	—	—	—	58
	5638.26	4.22	−0.720	—	84	—	106	—
	5691.50	4.30	−1.370	85	51	—	74	104
	5705.47	4.30	−1.360	—	46	—	59	93
	5717.83	4.28	−0.979	116	—	122	—	—
	5806.73	4.61	−0.900	—	—	—	65	99
	5814.81	4.28	−1.820	—	—	—	—	62
	5852.22	4.55	−1.180	—	63	78	70	95
	5883.82	3.96	−1.210	94	—	—	101	—
	5916.25	2.45	−2.990	104	—	—	—	—
	5934.65	3.93	−1.020	120	—	142	117	140
	6024.06	4.55	−0.060	—	102	—	—	—
	6027.05	4.08	−1.090	—	72	—	—	—
	6056.01	4.73	−0.400	—	91	—	—	123
	6065.48	2.61	−1.530	—	151	—	—	—
	6096.66	3.98	−1.780	—	62	95	71	83
	6151.62	2.18	−3.290	—	79	—	—	—
	6157.73	4.08	−1.110	120	95	—	102	120

Table 6, continued.

				Equivalent Widths (mÅ)				
				Star				
Element	λ (Å)	χ(eV)	log gf	1534	1616	1349	784	663
Fe I	6165.36	4.14	−1.470	—	56	—	75	97
	6173.34	2.22	−2.880	—	98	—	—	145
	6187.99	3.94	−1.570	—	—	—	81	102
	6200.31	2.60	−2.440	—	111	145	126	—
	6265.13	2.18	−2.550	155	—	—	143	—
	6380.74	4.19	−1.320	—	75	—	—	119
	6392.54	2.28	−4.030	—	—	—	65	84
	6411.65	3.65	−0.660	—	145	—	157	—
	6421.35	2.28	−2.010	—	133	—	—	—
	6430.85	2.18	−2.010	—	148	—	—	—
	6436.41	4.19	−2.460	—	—	—	21	42
	6469.19	4.83	−0.620	70	82	102	99	117
	6551.68	0.99	−5.790	—	—	56	41	65
	6591.31	4.59	−2.070	—	—	—	23	—
	6593.87	2.44	−2.420	137	—	—	—	—
	6597.56	4.79	−0.920	52	40	—	62	73
	6608.03	2.28	−4.030	—	40	—	66	76
	6609.11	2.56	−2.690	—	—	140	—	—
	6646.93	2.61	−3.990	41	—	—	—	63
	6703.57	2.76	−3.160	—	—	66	79	—
	6739.52	1.56	−4.950	—	—	—	70	48
	6750.15	2.42	−2.620	—	—	150	—	—
	6752.71	4.64	−1.200	—	38	86	73	101
	6806.85	2.73	−3.210	—	59	90	87	104
	6810.26	4.61	−0.990	—	—	98	91	94
	6820.37	4.64	−1.170	—	58	65	—	83
	6858.15	4.61	−0.930	—	65	—	—	103
	7130.92	4.22	−0.700	—	—	—	130	—
	7132.99	4.08	−1.610	—	—	77	64	90
Fe II	5425.25	3.20	−3.210	—	—	—	69	—
	5534.83	3.25	−2.770	—	87	—	102	—
	6084.10	3.20	−3.800	—	25	—	—	—
	6149.25	3.89	−2.720	73	54	80	63	—
	6247.55	3.89	−2.340	—	68	—	82	73
	6416.92	3.89	−2.680	78	63	69	59	56
	6432.68	2.89	−3.580	—	—	—	68	53

Table 7: Other lines studied.

					Equivalent Widths (mÅ)				
					Star				
Element	λ	χ(eV)	$\log gf$	Ref	769	806	1110	1118	395
Na I	6154.22	2.10	−1.51	PS	59	17	63	72	55
Na I	6160.75	2.10	−1.21	R03	89	—	72	86	78
Mg I	4730.04	4.34	−2.39	R03	81	—	—	—	—
Mg I	5711.10	4.34	−1.75	R99	115	77	107	—	—
Mg I	6318.71	5.11	−1.94	Ca07	—	—	45	58	55
Mg I	6965.41	5.75	−1.72	MR94	—	—	—	43	40
Mg I	7387.70	5.75	−0.87	MR94	85	—	105	—	80
Mg I	8717.83	5.91	−0.97	WSM	62	—	—	83	—
Mg I	8736.04	5.94	−0.34	WSM	—	—	—	128	—
Si I	5793.08	4.93	−2.06	R03	52	17	—	61	63
Si I	6125.03	5.61	−1.54	E93	44	24	29	39	42
Si I	6131.58	5.62	−1.68	E93	—	14	—	—	—
Si I	6155.14	5.62	−0.77	E93	91	77	—	87	89
Si I	7800.00	6.18	−0.72	E93	69	—	58	—	68
Si I	8728.01	6.18	−0.36	E93	89	—	—	—	—
Ca I	6102.73	1.88	−0.79	D2002	—	—	—	149	141
Ca I	6161.30	2.52	−1.27	E93	93	—	78	92	97
Ca I	6166.44	2.52	−1.14	R03	83	43	88	99	86
Ca I	6169.04	2.52	−0.80	R03	114	—	93	113	112
Ca I	6169.56	2.53	−0.48	DS91	126	—	121	125	127
Ca I	6455.60	2.51	−1.29	R03	79	—	71	—	89
Ca I	6471.66	2.51	−0.69	S86	132	98	—	—	125
Ca I	6493.79	2.52	−0.11	DS91	152	—	—	—	—
Ti I	4534.78	0.84	0.280	D2002	149	—	—	—	—
Ti I	4758.12	2.25	0.420	MFK	80	—	—	—	—
Ti I	4759.28	2.25	0.514	MFK	81	—	—	—	—
Ti I	4820.41	1.50	−0.439	MFK	83	—	—	—	83
Ti I	4999.51	0.83	0.250	MFK	—	—	119	—	—
Ti I	5009.66	0.02	−2.259	MFK	—	—	—	71	—
Ti I	5022.87	0.83	−0.434	MFK	—	—	—	—	109
Ti I	5039.96	0.02	−1.130	MFK	118	—	96	—	—
Ti I	5043.59	0.84	−1.733	MFK	63	—	—	—	—
Ti I	5087.06	1.43	−0.840	E93	60	—	—	56	56
Ti I	5113.45	1.44	−0.880	E93	—	—	—	59	—
Ti I	5145.47	1.46	−0.574	MFK	82	—	62	—	67
Ti I	5147.48	0.00	−2.012	MFK	82	—	—	97	94
Ti I	5173.75	0.00	−1.120	MFK	—	—	—	136	—
Ti I	5210.39	0.05	−0.883	MFK	—	—	102	—	—
Ti I	5219.71	0.02	−2.292	MFK	81	—	—	—	79
Ti I	5223.63	2.09	−0.559	MFK	—	—	29	—	—
Ti I	5295.78	1.05	−1.633	MFK	—	—	—	39	44
Ti I	5490.16	1.46	−0.937	MFK	70	—	—	—	—
Ti I	5689.48	2.30	−0.469	MFK	34	—	35	—	40
Ti I	5866.46	1.07	−0.871	E93	—	—	77	82	93
Ti I	5922.12	1.05	−1.465	MFK	62	—	—	59	—
Ti I	5978.55	1.87	−0.496	MFK	63	—	52	50	—
Ti I	6091.18	2.27	−0.370	R03	43	—	—	42	—

Table 7, continued.

					Equivalent Widths (mÅ)				
					Star				
Element	λ	χ(eV)	$\log gf$	Ref	769	806	1110	1118	395
Ti I	6126.22	1.07	−1.370	R03	61	10	45	—	60
Ti I	6258.11	1.44	−0.355	MFK	99	—	81	81	—
Ti I	6261.11	1.43	−0.480	B86	96	—	76	83	89
Ti I	6554.24	1.44	−1.219	MFK	—	—	—	55	—
Cr I	4836.85	3.10	−1.137	MFK	40	—	—	—	32
Cr I	5200.18	3.38	−0.650	MFK	40	—	—	—	—
Cr I	5296.70	0.98	−1.390	GS	133	82	—	134	132
Cr I	5304.18	3.46	−0.692	MFK	35	—	—	—	—
Cr I	5345.81	1.00	−0.980	GS	—	145	140	—	—
Cr I	5348.32	1.00	−1.290	GS	—	85	118	135	147
Cr I	5783.07	3.32	−0.500	MFK	49	—	47	60	62
Cr I	5783.87	3.32	−0.290	GS	74	—	64	68	76
Cr I	5787.93	3.32	−0.080	GS	71	—	69	—	70
Cr I	6330.09	0.94	−2.920	R03	—	—	58	61	70
Ni I	4904.42	3.54	−0.170	MFK	116	—	102	100	—
Ni I	4935.83	3.94	−0.360	MFK	82	—	60	85	—
Ni I	4953.21	3.74	−0.660	MFK	87	—	—	72	81
Ni I	4967.52	3.80	−1.570	MFK	40	—	—	—	—
Ni I	5010.94	3.63	−0.870	MFK	—	—	62	73	63
Ni I	5084.11	3.68	−0.180	E93	100	—	86	—	95
Ni I	5094.42	3.83	−1.080	MFK	51	—	38	—	—
Ni I	5115.40	3.83	−0.280	R03	101	—	—	—	90
Ni I	5157.98	3.61	−1.590	MFK	—	—	33	—	—
Ni I	5578.73	1.68	−2.640	MFK	93	—	—	—	91
Ni I	5589.37	3.90	−1.140	MFK	42	—	35	45	37
Ni I	5593.75	3.90	−0.840	MFK	56	—	—	61	68
Ni I	5760.84	4.11	−0.800	MFK	68	—	—	63	—
Ni I	5805.23	4.17	−0.640	MFK	56	37	—	—	52
Ni I	5996.74	4.24	−1.060	MFK	30	—	—	—	30
Ni I	6053.69	4.24	−1.070	MFK	—	—	—	39	—
Ni I	6086.29	4.27	−0.510	MFK	66	—	43	66	66
Ni I	6108.12	1.68	−2.440	MFK	106	—	90	—	—
Ni I	6111.08	4.09	−0.870	MFK	68	—	48	49	—
Ni I	6128.98	1.68	−3.320	MFK	66	—	51	—	—
Ni I	6176.82	4.09	−0.264	R03	—	—	—	77	—
Ni I	6186.72	4.11	−0.960	MFK	48	—	40	46	—
Ni I	6204.61	4.09	−1.150	MFK	52	—	23	—	42
Ni I	6223.99	4.11	−0.980	MFK	—	—	—	—	41
Ni I	6230.10	4.11	−1.260	MFK	40	—	—	26	37
Ni I	6322.17	4.15	−1.170	MFK	33	—	31	—	—
Ni I	6327.60	1.68	−3.150	MFK	84	—	—	79	81
Ni I	6378.26	4.15	−0.900	MFK	60	—	—	—	44
Ni I	6482.81	1.94	−2.630	MFK	—	35	—	—	—
Ni I	6532.88	1.94	−3.390	MFK	62	—	—	—	—
Ni I	6586.32	1.95	−2.810	MFK	74	—	71	92	—
Ni I	6635.14	4.42	−0.830	MFK	—	—	27	—	—
Ni I	6643.64	1.68	−2.030	MFK	142	—	109	150	136
Ni I	6767.78	1.83	−2.170	MFK	111	76	100	118	113

Table 7, continued.

					Equivalent Widths (mÅ)				
					Star				
Element	λ	χ(eV)	$\log gf$	Ref	769	806	1110	1118	395
Ni I	6772.32	3.66	−0.970	R03	—	—	55	79	—
Ni I	6842.04	3.66	−1.477	E93	49	—	—	42	53
Ni I	7788.93	1.95	−1.990	E93	—	—	—	—	122

References: B86: Blackwell D.E. et al. (1986); Ca07: Carretta et al. (2007);
D2002; Depagne et al. (2002); DS91: Drake & Smith (1991);
E93: Edvardsson et al. (1993); GS: Gratton & Sneden (1988);
MFK: Martin et al., (2002); MR94: Mcwilliam & Rich (1994);
PS: Preston & Sneden (2001); R03: Reddy et al. (2003);
R99: Reddy et al. (1999); WSM: Wiese, Smith & Miles (1969).

Table 8: Other lines studied.

					Equivalent Widths (mÅ)				
					Star				
Element	λ	χ(eV)	$\log gf$	Ref	1534	1616	1349	784	663
Na I	6154.22	2.10	−1.51	PS	47	68	—	68	105
Na I	6160.75	2.10	−1.21	R03	—	—	—	86	122
Mg I	4730.04	4.34	−2.39	R03	88	—	—	79	—
Mg I	5711.10	4.34	−1.75	R99	140	124	124	138	152
Mg I	6318.71	5.11	−1.94	Ca07	—	58	—	74	91
Mg I	7387.70	5.75	−0.87	MR94	—	102	98	113	120
Mg I	8736.04	5.94	−0.34	WSM	133	—	—	—	—
Al I	6698.67	3.14	−1.63	R03	—	—	58	—	—
Al I	7835.32	4.04	−0.58	R03	—	39	—	69	78
Al I	7836.13	4.02	−0.40	R03	—	42	—	80	102
Al I	8772.88	4.02	−0.25	R03	99	—	99	—	—
Al I	8773.91	4.02	−0.07	R03	114	—	—	—	140
Si I	5793.08	4.93	−2.06	R03	53	32	48	76	86
Si I	6125.03	5.61	−1.54	E93	31	26	—	50	—
Si I	6145.02	5.61	−1.43	E93	—	—	—	59	64
Si I	6155.14	5.62	−0.77	E93	79	81	—	96	—
Si I	7800.00	6.18	−0.72	E93	40	—	—	75	—
Si I	8728.01	6.18	−0.36	E93	75	—	—	—	122
Si I	8742.45	5.87	−0.51	E93	—	—	106	—	119
Ca I	6102.73	1.88	−0.79	D2002	—	—	—	160	—
Ca I	6161.30	2.52	−1.27	E93	82	—	—	101	137
Ca I	6166.44	2.52	−1.14	R03	95	80	118	101	128
Ca I	6169.04	2.52	−0.80	R03	—	—	—	114	—
Ca I	6169.56	2.53	−0.48	DS91	—	—	—	142	—
Ca I	6455.60	2.51	−1.29	R03	—	80	101	90	—
Ca I	6471.66	2.51	−0.69	S86	122	114	—	—	—
Ca I	6493.79	2.52	−0.11	DS91	144	—	—	—	—
Ti I	4759.28	2.25	0.514	MFK	—	86	—	88	—
Ti I	4820.41	1.50	−0.439	MFK	—	65	—	92	—
Ti I	5009.66	0.02	−2.259	MFK	—	—	112	88	—
Ti I	5039.96	0.02	−1.130	MFK	—	123	—	—	—
Ti I	5043.59	0.84	−1.733	MFK	—	—	73	—	111
Ti I	5062.10	2.16	−0.464	MFK	35	—	—	—	64
Ti I	5113.45	1.44	−0.880	E93	—	—	—	—	106
Ti I	5147.48	0.00	−2.012	MFK	—	89	—	—	—
Ti I	5210.39	0.05	−0.883	MFK	—	—	—	156	—
Ti I	5219.71	0.02	−2.292	MFK	—	—	117	—	—
Ti I	5295.78	1.05	−1.633	MFK	—	36	—	56	64
Ti I	5689.48	2.30	−0.469	MFK	—	—	—	38	67
Ti I	5866.46	1.07	−0.871	E93	—	91	—	—	155
Ti I	5922.12	1.05	−1.465	MFK	—	—	—	—	101
Ti I	5978.55	1.87	−0.496	MFK	—	43	—	76	—
Ti I	6126.22	1.07	−1.370	R03	—	44	—	71	—
Ti I	6258.11	1.44	−0.355	MFK	—	96	—	—	149
Ti I	6261.11	1.43	−0.480	B86	95	86	124	105	—
Ti I	6554.24	1.44	−1.219	MFK	—	—	—	51	84

Table 8, continued.

					Equivalent Widths (mÅ)				
					Star				
Element	λ	χ(eV)	$\log gf$	Ref	1534	1616	1349	784	663
Cr I	4836.85	3.10	−1.137	MFK	—	—	49	—	—
Cr I	5193.50	3.42	−0.720	MFK	—	—	—	23	—
Cr I	5196.45	3.45	−0.270	MFK	—	—	92	—	—
Cr I	5214.13	3.37	−0.740	MFK	—	—	—	32	—
Cr I	5296.70	0.98	−1.390	GS	—	129	—	—	—
Cr I	5348.32	1.00	−1.290	GS	—	126	—	154	—
Cr I	5702.32	3.45	−0.666	MFK	21	—	63	—	—
Cr I	5783.07	3.32	−0.500	MFK	—	—	—	54	75
Cr I	5783.87	3.32	−0.290	GS	49	60	95	57	90
Cr I	5787.92	3.32	−0.080	GS	51	—	100	—	103
Cr I	6330.09	0.94	−2.920	R03	—	67	—	—	—
Ni I	4904.42	3.54	−0.170	MFK	117	—	139	—	—
Ni I	4935.83	3.94	−0.360	MFK	—	—	99	78	—
Ni I	4953.21	3.74	−0.660	MFK	61	65	—	—	105
Ni I	4967.52	3.80	−1.570	MFK	—	—	—	35	—
Ni I	5010.94	3.63	−0.870	MFK	—	—	78	68	—
Ni I	5048.85	3.85	−0.370	MFK	94	—	—	—	—
Ni I	5084.11	3.68	−0.180	E93	—	94	—	—	—
Ni I	5094.42	3.83	−1.080	MFK	51	53	—	—	—
Ni I	5115.40	3.83	−0.280	R03	—	95	—	—	—
Ni I	5157.98	3.61	−1.590	MFK	—	—	44	—	—
Ni I	5578.73	1.68	−2.640	MFK	—	—	—	105	—
Ni I	5589.37	3.90	−1.140	MFK	—	—	46	—	—
Ni I	5593.75	3.90	−0.840	MFK	—	51	68	—	84
Ni I	5643.09	4.17	−1.250	MFK	—	—	27	—	—
Ni I	5748.36	1.68	−3.260	MFK	—	64	—	—	113
Ni I	5760.84	4.11	−0.800	MFK	—	59	61	—	—
Ni I	5805.23	4.17	−0.640	MFK	—	—	—	—	59
Ni I	5996.74	4.24	−1.060	MFK	—	—	—	—	57
Ni I	6086.29	4.27	−0.510	MFK	—	—	—	77	—
Ni I	6108.12	1.68	−2.440	MFK	124	90	140	—	—
Ni I	6111.08	4.09	−0.870	MFK	—	—	—	—	75
Ni I	6128.98	1.68	−3.320	MFK	—	48	—	69	105
Ni I	6176.82	4.09	−0.264	R03	—	—	—	86	114
Ni I	6177.25	1.83	−3.510	MFK	—	—	—	45	67
Ni I	6186.72	4.11	−0.960	MFK	38	—	—	46	—
Ni I	6204.61	4.09	−1.150	MFK	—	34	—	49	56
Ni I	6223.99	4.11	−0.980	MFK	—	—	—	50	—
Ni I	6230.10	4.11	−1.260	MFK	—	27	—	—	—
Ni I	6327.60	1.68	−3.150	MFK	60	74	—	93	99
Ni I	6482.81	1.94	−2.630	MFK	—	82	112	96	—
Ni I	6586.32	1.95	−2.810	MFK	76	—	92	76	—
Ni I	6635.14	4.42	−0.830	MFK	—	—	—	31	43
Ni I	6643.64	1.68	−2.030	MFK	—	129	—	139	—
Ni I	6767.78	1.83	−2.170	MFK	131	—	—	—	155

Table 8, continued.

					Equivalent Widths (mÅ)				
					Star				
Element	λ	χ(eV)	$\log gf$	Ref	1534	1616	1349	784	663
Ni I	6772.32	3.66	−0.970	R03	—	—	—	91	90
Ni I	7788.93	1.95	−1.990	E93	—	118	156	142	—

References: B86: Blackwell D.E. et al. (1986); Ca07: Carretta et al. (2007);
D2002; Depagne et al. (2002); DS91: Drake & Smith (1991);
E93: Edvardsson et al. (1993); GS: Gratton & Sneden (1988);
MFK: Martin et al., (2002); MR94: Mcwilliam & Rich (1994);
PS: Preston & Sneden (2001); R03: Reddy et al. (2003);
R99: Reddy et al. (1999); WSM: Wiese, Smith & Miles (1969).

Table 9: Atmospheric parameters from photometry (ph) and spectroscopy (sp).

ID	$T_{\rm eff,ph}$ (K)	log g_{ph} dex	$T_{\rm eff,sp}$ (K)	log g_{sp} dex	ξ km s^{-1}	$[FeI/H]\pm\sigma$ (#)	$[FeII/H]\pm\sigma$ (#)	Comment
395	5205	2.74	5100	2.7	1.6	−0.15±0.15(53)	−0.15±0.12(5)	Member
663	5123	2.85	4900	3.2	2.3	0.07±0.14(37)	0.06±0.13(3)	Member
769	5196	2.53	5200	3.0	1.3	0.10±0.14(53)	0.08±0.17(3)	Member
784	4955	2.82	5000	2.5	1.7	−0.08±0.13(39)	−0.11±0.12(6)	Non-Member
806	6324	2.86	6000	2.7	4.9	−0.53±0.12(20)	−0.52(2)	Non-Member/binary Cepheid?
1110	5161	2.68	5350	3.4	1.0	0.03±0.15(44)	0.01±0.09(6)	Member
1118	4958	2.63	5100	2.6	1.5	−0.16±0.12(44)	−0.17±0.10(3)	Member
1349	4796	2.72	5100	2.6	2.1	0.01±0.19(25)	0.01(2)	Member
1534	4982	2.73	5000	2.0	2.2	−0.30±0.16(15)	−0.29(2)	Non-Member
1616	5465	2.83	5450	3.5	1.7	−0.07±0.16(31)	−0.09±0.14(5)	Non-Member

Notes. For [Fe I/H] and [Fe II/H], we also show the standard deviation and the number of lines employed.

Table 10: Adopted solar abundances.

Element	This work	Grevesse & Sauval (1998)	Asplund et al. (2009)
Fe	7.50	7.50	7.50
Na	6.26	6.33	6.24
Mg	7.55	7.58	7.60
Al	6.31	6.47	6.45
Si	7.61	7.55	7.51
Ca	6.37	6.36	6.34
Ti	4.93	5.02	4.95
Cr	5.65	5.67	5.64
Ni	6.29	6.25	6.22
Y	2.04	2.24	2.21
Ba	2.18	2.13	2.18
Ce	1.48	1.58	1.58
Nd	1.42	1.50	1.42

Table 11: Abundance Ratios ($[X/Fe]$) for the elements from Na to Cr for the stars observed.

Cluster giants							
ID	[Na/Fe]NLTE	[Mg/Fe]	[Al/Fe]	[Si/Fe]	[Ca/Fe]	[Ti/Fe]	[Cr/Fe]
395	+0.15(2)	+0.10±0.13(3)	—	+0.13±0.09(4)	+0.02±0.13(7)	+0.07(1)	+0.02±0.14(7)
663	+0.12(2)	+0.03±0.12(3)	+0.15±0.04(3)	+0.23±0.11(4)	−0.06(2)	+0.04±0.14(9)	−0.10±0.02(3)
769	+0.04(2)	−0.12±0.13(4)	—	−0.05±0.04(5)	−0.05±0.15(7)	+0.10±0.11(18)	+0.04±0.12(7)
1110	+0.13(2)	+0.03±0.14(3)	—	−0.14(2)	+0.04±0.11(5)	+0.09±0.13(11)	+0.18±0.06(6)
1118	+0.38(2)	+0.23±0.07(4)	—	+0.07±0.09(3)	+0.12±0.08(5)	+0.08±0.13(13)	+0.14±0.13(6)
1349	—	−0.11(2)	+0.16(2)	−0.19(2)	−0.01(2)	+0.28±0.11(4)	+0.30±0.09(5)
Tombaugh 1[a]	+0.17±0.06	+0.03±0.05	+0.15	+0.01±0.07	+0.01±0.03	+0.11±0.04	+0.10±0.06
Field stars							
ID	[Na/Fe]NLTE	[Mg/Fe]	[Al/Fe]	[Si/Fe]	[Ca/Fe]	[Ti/Fe]	[Cr/Fe]
784	+0.20(2)	+0.17±0.13(4)	+0.27(2)	+0.14±0.10(5)	−0.06±0.09(6)	+0.03±0.07(10)	−0.13±0.10(5)
806[b]	+0.27(1)	+0.02(1)	—	+0.14±0.11(4)	+0.05(2)	+0.32(1)	−0.12±0.08(3)
1534	+0.21(1)	+0.25±0.02(3)	—	−0.15±0.09(5)	−0.20±0.15(4)	+0.01(2)	−0.22±0.11(3)
1616	+0.34(1)	+0.18±0.03(3)	−0.10(2)	−0.21±0.08(3)	−0.01±0.06(3)	+0.27±0.13(10)	+0.17±0.14(4)

Notes. For all abundances ratios, we also show the standard deviation and the number of lines employed. [Na/Fe] accounts for the NLTE effects calculated as in Gratton et al. (1999), see text. (a) Mean abundance ratio for each element for Tombaugh 1. (b) The classical Cepheid XZ CMa.

Table 12: Abundance Ratios ($[X/Fe]$) for the elements from Ni to Nd for the stars observed.

Cluster giants					
ID	[Ni/Fe]	[Y/Fe]	[Ba/Fe]	[Ce/Fe]	[Nd/Fe]
395	−0.06±0.13(18)	−0.10(1)	+0.28(1)	+0.25(1)	+0.35(1)
663	−0.04±0.15(14)	+0.00(1)	—	—	—
769	+0.02±0.15(28)	+0.07(1)	+0.38(1)	+0.10(1)	+0.30(1)
1110	−0.05±0.13(19)	+0.14(1)	+0.37(1)	+0.37(1)	+0.47(1)
1118	+0.04±0.12(19)	+0.13(1)	+0.36(1)	+0.29(1)	—
1349	−0.14±0.09(12)	—	—	—	—
Tombaugh 1[a]	−0.04±0.02	+0.06±0.04	+0.35±0.03	+0.25±0.06	+0.37±0.05
Field stars					
ID	[Ni/Fe]	[Y/Fe]	[Ba/Fe]	[Ce/Fe]	[Nd/Fe]
784	−0.14±0.14(18)	+0.30(1)	−0.02(1)	+0.20(1)	+0.32(1)
806[b]	+0.20±0.16(3)	—	+0.73(1)	—	—
1534	−0.27±0.13(9)	−0.07(1)	−0.05(1)	—	—
1616	+0.02±0.13(15)	−0.11(1)	+0.39(1)	—	+0.04(1)

Notes. For all abundances ratios, we also show the standard deviation and the number of lines employed. (a) Mean abundance ratio for each element for Tombaugh 1. (b) The classical Cepheid XZ CMa.

Table 13: Abundance uncertainties for star 769.

Element	ΔT_{eff}	$\Delta \log g$	$\Delta\xi$	$\left(\sum \sigma^2\right)^{1/2}$
	+180 K	+0.3	+0.3 km s^{-1}	
Fe I	+0.14	0.00	−0.14	0.20
Fe II	−0.11	+0.19	−0.11	0.25
Na I	+0.12	−0.01	−0.05	0.13
Mg I	+0.09	−0.01	−0.07	0.11
Al I	+0.09	−0.04	−0.05	0.11
Si I	0.00	+0.05	−0.05	0.07
Ca I	+0.16	−0.04	−0.15	0.22
Ti I	+0.23	−0.02	−0.12	0.26
Cr I	+0.15	−0.02	−0.09	0.18
Ni I	+0.11	+0.03	−0.12	0.17
Y II	−0.02	+0.08	−0.05	0.10
Zr I	+0.01	−0.03	−0.06	0.07
Ba II	+0.12	+0.17	−0.14	0.25
Ce II	−0.02	+0.05	−0.10	0.11
Nd II	+0.05	+0.15	−0.05	0.17

Notes. Each column gives the variation of the abundance caused by the variation in $T_{\rm eff}$, $\log g$ and ξ. The last column gives the compounded rms uncertainty of the second to fourth columns. Abundance uncertainties of aluminium were calculated using the star 663.